HHS Public Access

Author manuscript

Neuron. Author manuscript; available in PMC 2024 September 20.

Published in final edited form as:

Neuron. 2023 September 20; 111(18): 2899–2917.e6. doi:10.1016/j.neuron.2023.06.006.

Toggling between food-seeking and self-preservation behaviors via hypothalamic response networks

Isabel de Araujo Salgado[1], **Chia Li**[1], **C Joseph Burnett**[1], **Shakira Rodriguez Gonzalez**[1], **Jordan J. Becker**[1], **Allison Horvath**[1], **Thomas Earnest**[2], **Alexxai V. Kravitz**[2], **Michael J. Krashes**[1,3,4]

[1]Diabetes, Endocrinology, and Obesity Branch, National Institute of Diabetes and Digestive and Kidney Diseases, National Institutes of Health, Bethesda, MD 20892, USA.

[2]Department of Psychiatry, Washington University School of Medicine, St Louis, MO, 63110, USA.

[3]National Institute on Drug Abuse (NIDA), National Institutes of Health, Baltimore, MD 21224, USA.

[4]Lead contact

Summary

Motivated behaviors are often studied in a vacuum to assess labeled lines of neural connections underlying innate actions. However, in nature, multiple systems compete for expression of goal-directed behaviors via complex neural networks. Here, we examined flexible survival decisions in animals tasked with food-seeking under predation threat. We found that predator exposure rapidly induced physiological, neuronal, and behavioral adaptations in mice highlighted by reduced food-seeking and consumption contingent on current threat level. Diminishing conflict via internal state or external environment perturbations shifted feeding strategies. Predator introduction and/or selective manipulation of danger-responsive cholecystokinin (Cck) cells of the dorsal premammilary nucleus (PMd) suppressed hunger-sensitive Agouti-related peptide (AgRP) neurons, providing a mechanism for threat-evoked hypophagia. Increased caloric need enhanced food-seeking under duress through AgRP pathways to the bed nucleus of the stria terminalis (BNST) and/or lateral hypothalamus (LH). Our results suggest oscillating interactions between systems underlying self-preservation and food-seeking to promote optimal behavior.

*Correspondence: michael.krashes@nih.gov.

Author contributions

I.A.S., C.J.B., S.R.G., and M.J.K. designed and conducted behavioral experiments. I.A.S., J.J.B., A.H. and M.J.K. performed immunohistochemistry. I.A.S., C.L., and C.J.B. performed surgeries for the experiments. I.A.S., C.J.B., S.R.G., and M.J.K. analyzed experimental data and performed statistical tests. T.E. and A.V.K. provided FED code and expertise to accurately assess feeding behavior. I.A.S. and M.J.K. wrote the manuscript with input from all the authors.

Declaration of interests

The authors declare no competing interests.

Data/Methods S1, Statistical analyses, related to Figures 1–7, S1–S8.

eTOC

Motivated behaviors are often studied in a behavioral vacuum for experimental simplicity. However, in nature, systems compete in real time for expression of goal-directed behaviors via complex neural networks. Here, de Araujo Salgado et al. examine flexible behaviors used by animals tasked with foodseeking under predation threat and uncover a neural mechanism of how these systems interact to maximize survival.

Introduction

Brain networks are designed to rapidly assess internal state, external environment, and learned associations to decisively select the best option[1–3]. When animals entertain conflicting incentives and only mutually exclusive courses of action will meet those demands, they are forced to make a choice[4]. Two of the most biologically relevant aspects of prey species are the motivation to obtain food and evade predation. To accurately detect, localize, and identify impending threat, mice rely on a repertoire of defense behaviors crafted from incoming sensory information. Self-preservation is imperative as prey are often forced to leave the safety of their dwellings to seek the necessary calories to ensure survival. This commutation between a predator encounter and food procurement requires real-time estimations, computations, and actions orchestrated by the brain to optimize behavior. The predation risk allocation hypothesis predicts that animals trade-off foraging efforts and vigilance in relation to the temporal variation of predation exposure, such that they meet their energy requirements while simultaneously minimizing liability of being harmed or killed[5]. However, few studies have substantiated this theory and a neural mechanism underlying this trade-off remains elusive.

To analyze this particular cost-benefit relationship, we modified classical paradigms whereby mice were obligated to jeopardize their safety to acquire food in the presence of a rat predator[6–10]. Unlike typically employed escape-eliciting fear stimuli that rely on a single sensory modality such as a loud sound[11], looming disc[12], odor[13], or mechanical predator[6], we used a freely moving, hungry rat[14–16] as an impediment to successful food acquisition. We found that this ethologically relevant compilation of perilous sensory cues acts in concert to rapidly induce physiological, behavioral, and neuronal alterations in mice.

Models of defensive responses to predation predict that rival motivations are constricted as a function of predatory imminence[17,18]. To determine the impact of threat on food-seeking, we used Feeding Experimentation Devices (FED3) that enable quantitative and qualitative information on the eatng patterns of mice based on precise timestamping of pre-weighed food pellet retrieval[19]. Our studies reveal rat introduction dynamically transforms food-seeking and consumption in hungry mice contingent on the current level of threat posed by the predator. Owing to the tunability of these hardwired survival systems, removal of the conflict drastically shifts behavior toward a single outcome.

The hypothalamus comprises evolutionary conserved brain networks for preserving physiological homeostasis and regulating survival actions[20,21]. Agouti-related peptide (AgRP) neurons of the arcuate nucleus (ARC) are major contributors to energy

balance[22–26] bidirectionally modulating feeding behavior through parallel, redundant signaling pathways[27–30]. AgRP activity is rapidly and durably suppressed by the anticipation and consumption of calories, respectively[31–35]. Although the contribution of AgRP cells to appetite regulation is undisputed, it is unknown how this population responds to and orchestrates actions under stress, such as foraging under duress of an imminent threat. We found that exposure to a rat predator in the absence of food inhibits AgRP neurons as a mechanism to mitigate food seeking during danger. Furthermore, AgRP activity via communication to the bed nucleus of the stria terminalis (BNST) and/or lateral hypothalamus (LH) was both required and permissive to food-seek under periods of predation.

The hypothalamic medial zone, encompassing the highly interconnected anterior hypothalamic nucleus (AH), dorsal medial part of the ventromedial nucleus (VMHdm), and dorsal premammillary nucleus (PMd), is critical for the expression of defensive behaviors[14–16,36–39]. Chemical lesions of the PMd severely limited the expression of escape and freezing in response to a predator[36] while recent interventions of PMd neurons reinforced their role in coordinating escape and flight from myriad threats[14–16,39–43]. Congruently, we established high levels of neural activity in the PMd, enriched by the molecular marker cholecystokinin (Cck), in response to a rat predator interaction. Although not endogenously regulated by hunger state, PMd^{Cck} neural inhibition supplemented food intake during rat exposure while stimulation attenuated consumption in the absence of threat. We identified a mechanism for this appetite control as acute activation of predator-sensitive PMd^{Cck} neurons suppressed AgRP activity reproducing the inhibition observed during predator presentation.

Results

A rat predator stimulus evokes physiological, behavioral and neuronal changes in mice

Sensory information pertaining to threat leads to a multitude of peripheral and central defensive reactions. Mammalian prey species need to quickly adapt to predator cues for survival. To investigate these responses, we presented mice with either a stuffed rat plushy as a control or a freely moving, hungry rat (Figure 1A). The rat predator stimulus resulted in both elevated fecal output (Figure 1B) and time spent immobile (Figure 1C), two behavioral responses displayed by mice under states of stress/fear, compared to the stuffed animal. Blood samples revealed predator-exposed mice had higher levels of the stress hormone corticosterone than age- and sex-matched controls presented with the stuffed animal (Figure 1D). A major source of the hypothalamic-pituitary-adrenal axis resulting in corticosterone release emanates from corticotropin-releasing hormone (CRH) neurons residing in the paraventricular nucleus of the hypothalamus (PVH). To evaluate whether these PVH^{CRH} cells were responsive to impending danger, we recorded real-time population dynamics by targeting the genetically-encoded calcium indicator GCaMP to this region in a Cre-dependent fashion (Figure 1E). While experimenter intervention (opening the cage top) transiently increased PVH^{CRH} population activity, this rise rapidly returned to baseline after the addition of a stuffed animal (Figure 1F). On the contrary, exposure to a rat predator led to a robust and durable increase in PVH^{CRH} network dynamics (Figure 1F–G).

Concordantly, higher levels of Fos expression, a proxy for neural activity, were observed in the PVH, as well as the paraventricular thalamus (PVT), central amygdala (CeA), lateral amygdala (LA) and dorsal premammillary nucleus (PMd) when mice were exposed to a rat predator compared to a stuffed animal (Figure S1). Increased Fos staining was also detected in the basal lateral amygdala (BLA), dorsal medial region of the ventromedial hypothalamic nucleus (dmVMH), dorsal and ventral regions of both the bed nucleus of the stria terminalis (dBNST and vBNST) and periaqueductal grey (dPAG and vPAG) and lateral parabrachial nucleus (lPBN) in mice exposed to the rat predator versus stuffed animal although these differences failed to reach significance (Figure S1).

To examine the putative physiological adaptations under autonomic control in response to threat, we measured mean arterial blood pressure, heart rate and core body temperature using telemetry probes in mice presented sequentially with a stuffed animal followed by a rat predator (Figure 1H–J). Importantly, a sufficient period was given between stimuli presentation to allow a return to baseline levels. Rat predator exposure significantly heightened mean arterial blood pressure (Figure1H), heart rate (Figure1I) and core body temperature compared to the stuffed animal trial (Figure1J). Importantly, these changes were independent of total activity (Figure1K). Collectively, these experiments establish that rat predator exposure elicits the physiological, behavioral, and neuronal changes expected from a strong stressor stimulus.

A rat predator stimulus reduces food seeking and consumption in hungry mice

To evaluate the intersection between self-preservation and caloric need, feeding behavior was assessed in overnight fasted mice under four discrete conditions: when the adjacent cage is 1) empty, or contains 2) a stuffed rat animal, 3) 2,3,5-trimethyl-3-thiazoline (TMT) or 4) a rat predator (Figure 2A). After a 20 min acclimation period whereby food is unavailable, mice were then provided with *ad libitum* access to individually delivered 20mg grain pellets from a Feeding Experimental Device during a 20 min trial phase in each condition (Figure S2A). This was followed by a 20 min post phase when the various stimuli were removed from the adjacent cage but food access remained (Figure S2A). While the amount of food intake was comparable between the empty cage and stuffed rat conditions, TMT exposure diminished caloric consumption, an effect that was exacerbated in the rat predator condition (Figure 2B–C). Time-locked feeding events (Figure 2B) revealed this suppression of food intake was at least in part due to increased latency to acquire the first pellet during the trial phase, with a number of subjects failing to procure a single pellet in the predator condition until the rat stimulus was removed (Figure 2D), suggesting high threat levels delay the initiation of feeding. Cumulative feeding curves (Figure 2E) and binned eating events (Figure 2F) demonstrated that distinct stimuli determined feeding rates. On average, mice ate at a faster rate during the early stages of the trial phase in the empty cage condition and this peak was progressively delayed in the stuffed rat, TMT and rat predator conditions (Figure 2E–F). Notably, maximum feeding events in the predator condition were observed after the rat was extracted in the post phase (Figure 2E–F).

Interpellet interval (IPI) or the time elapsed between each pellet retrieval and consummatory event can provide critical information about the microstructure of feeding. Smaller IPIs

imply fewer distractors to interrupt feeding bouts while longer IPIs may arise due to environmental contexts that serve to reprioritize behavior. In both the empty cage and stuffed rat conditions, we found that the majority of pellets procured and ingested occurred with an IPI of 30 seconds or less (66.2% and 55.6%, respectively; Figure 2G–H) while the minority was obtained with an IPI of 60 seconds or greater (19.9% and 28.5%, respectively; Figure 2G–H). Moreover, even though mice in the TMT condition exhibited an overall decrease in cumulative food intake highlighted by an increased latency to procure the first pellet and slower rate of consumption (Figure 2B–F), they manifested a comparable IPI as the empty cage and stuffed rat conditions with 68.8% of pellets consumed with an IPI of 30 seconds or less and 21.5% with an IPI of 60 seconds or more (Figure 2I). In contrast, only a fraction of pellets were procured and ingested with an IPI of 30 seconds or less (15.4%) in the rat predator condition where the majority of pellets were retrieved with an IPI of 60 seconds or greater (61.5%; Figure 2J). Video tracking supported these IPI analyses as mice in the empty cage, stuffed rat and TMT conditions spent significantly more time in the quadrant housing the FED than the rat predator condition (Figure S2B). Further reinforcing the context-dependent foraging strategies, we found that meal number (Figure S2C) and the number of pellets per meal (Figure S2D) were attenuated in the rat predator condition.

Food seeking and consumption strategy in hungry mice rapidly transforms after threat removal

We observed that mice exposed to a rat predator displayed a higher amount of food intake during the post phase after the stimulus was removed (Figure S2E). The number of pellets consumed during the trial and post phases was significantly correlated across conditions (Figure S2F) resulting in comparable total (trial + post) food intake between each context (Figure S2G). To measure the dynamic switch in food seeking and consumption, we compared feeding behaviors of mice exposed to a rat predator (trial phase) and after it was removed (post phase). Total intake was significantly increased following the extraction of the rat predator (Figure S2H). Cumulative feeding curves and binned eating events showed that mice ate at a higher rate in the absence of the rat during the post phase compared to the trial phase when the rat was present (Figure S2I–J). Similarly, the IPI underwent a substantial shift between the trial phase and post phase in both pellets obtained with an IPI of 30 seconds or less (15.4% vs 70.1%, respectively) and an IPI of 60 seconds or greater (61.5% vs 24.4%; Figure S2K). Accordingly, meal number (Figure S2L) and number of pellets per meal (Figure S2M) were elevated in the post compared to trial phase.

Hungry mice fail to habituate or adapt to a rat predator stimulus

Next, we sought to determine if hungry mice were able to adapt/habituate to the various stimuli with repetition either through a dampening of stimuli intensity or novelty. Each animal was exposed to the different conditions across four separate trials and feeding behavior was measured as a proxy for adaptation and/or habituation. While no changes in total caloric consumption or patterns of food intake were seen in the empty cage or stuffed rat condition, we observed a rise in food intake in mice exposed to TMT across trials (Figure S3A–B), a result of a reduced latency to initiate feeding (Figure S3C) and faster rate of consumption (Figure S3D–E). Notably, despite 4 separate exposures to the rat predator,

food intake remained heavily suppressed across trials accentuating the profound effect of a natural fear stimulus (Figure S3A–E).

Diminishing conflict alters feeding behavior

To further gauge choice behavior, experiments were conducted whereby one of these conflicts was minimized by changing the internal state of the animal or moving the location of the FED (Figure 3A). Hungry mice tasked with procuring food from the FED positioned in the threat zone (TZ) adjacent to the rat chamber exhibited comparable levels of food consumption observed in experiments above, with a handful of animals never acquiring a single pellet (Figure 3B, Figure S4A; Fasted-TZ). The number of pellets consumed was further reduced when sated mice were tested with the FED in the TZ (Figure 3B, Figure S4A; Sated-TZ). However, food intake was escalated in hungry mice when the FED was repositioned behind the hide wall in the safe zone (SZ) on the opposite side of the rat chamber (Figure 3B, Figure S4A; Fasted-SZ). Reducing either caloric need or pending threat drastically shaped feeding patterns. Fasted-SZ mice displayed a higher rate of consumption and shorter latency to procure the first pellet than both Fasted-TZ and Sated-TZ conditions (Figure 3C–E). The majority of pellets were consumed with an IPI of 60 seconds or greater (56.1%) and only a fraction was procured with an IPI of 30 seconds or less (19.5%) in the Fasted-TZ condition (Figure 3F). This was reversed in the Fasted-SZ condition where the bulk of pellets were retrieved with an IPI of 30 seconds (67.3%) versus the minority with an IPI of 60 seconds or more (29.2%) (Figure 3F). Consequently, meal number (Figure S4B) and number of pellets per meal (Figure S4C) were enhanced in the Fasted-SZ versus the Fasted-TZ and Sated-TZ conditions. Thus, the location of the food source as well as the internal state of the animal determines not only the quantitative, but the qualitative, value of food consumed.

The spatial position of the rat predator strongly influences feeding responses in mice

Matching the feeding patterns, mice in the Fasted-TZ condition spent a higher amount of time in the TZ abutting the rat chamber and lower amount of time in the SZ behind the hide wall than the Fasted-SZ and Sated-TZ conditions (Figure 3G–H, Figure S4D). This tracking data suggests the interaction between FED position and rat predator is critical in governing food-seeking behavior. To understand this interplay on a more nuanced level, the rat’s spatial position in the adjacent chamber was scored during each pellet retrieval. We found that only 14% of all pellets (7 of 53) consumed by Fasted-TZ mice were done so when the snout of the rat was inside the nearest quadrant to the FED, despite the rat spending nearly half (43%) of the entire trial time in this quadrant (Figure 3I). To further investigate this relationship, hungry mice were tasked with food-seeking under no threat (empty cage) or when the rat was positioned at the farthest versus nearest point to the FED (Figure 3J). Animals in the empty cage and “rat far away” conditions exhibited comparable total food intake, latency to initiate feeding, and time spent in the TZ and SZ (Figure 3K–M, Figure S4E). However, the number of pellets consumed and time spent in the TZ were reduced, while the latency to consume the first pellet and time spent in the SZ were elevated in the “rat near” condition (Figure 3K–M, Figure S4E). This suggests mice rapidly compute risk versus reward, maximizing food seeking behavior when threat levels are lowest.

Rat predator visual cues are not required to suppress feeding in mice

Since both repositioning the FED to the safe zone behind the hide wall or constraining the rat to a distant location from the FED alleviated food intake suppression, we reasoned that vision was a critical sensory modality encoding this choice behavior. To directly examine this, a cohort of mice were tested in complete darkness with the FED in the threat zone. This may be more ethologically relevant as both mice and rats are nocturnal and often rely on olfactory and auditory cues to pinpoint food sources and avoid danger. Despite eliminating sight, the presence of the rat predator was still sufficient to curtail food consumption (Figure S4F), implying that alternative sensory pathways are sufficient to signal threat and attenuate feeding behavior.

AgRP activity is rapidly blunted during rat predator exposure

Our experiments demonstrate that the presence of a rat predator suppresses feeding behavior. Given the role of AgRP neurons in mediating foraging and food intake we posited that exposure to threat could inhibit these cells. To investigate this possibility, fasted mice expressing GFP specifically in AgRP/NPY labeled neurons[44,45] were co-stained for Fos protein. Hungry animals exposed to a rat predator exhibited significantly lower levels of co-labeled AgRP/Fos cells than those exposed to a stuffed rat, a condition that failed to alter food intake (Figure 4A–C). This suggests that AgRP inhibition may serve as a potential mechanism for the diminished feeding behavior observed in the presence of a rat predator. To test this *in vivo*, we recorded real-time population dynamics of AgRP neurons in fasted mice via targeted GCaMP expression to the ARC (Figure 4D–E). While the addition of a stuffed rat, in the absence of food, had no effect on activity, the presence of a rat predator reduced AgRP network responses (Figure 4E–H). Interestingly, while food availability completely suppressed AgRP activity when the stuffed rat remained in the cage, it failed to do so with the rat predator still present (Figure 4F–G,I). This partial reduction of AgRP activity to food observed in the rat predator condition was likely due to fewer feeding events compared to the stuffed rat condition (Figure 2A–C). Reinforcing this notion, removal of the rat predator further inhibited AgRP dynamics as feeding events increased (Figure 4F–G, 2B,E–F). In a parallel set of recordings, we found that similar to food presentation[33] the predator-evoked suppression of AgRP neurons was reversible after the threat was extracted from the cage (Figure S5A–D). Additionally, we demonstrated that the rat stimulus failed to further reduce AgRP population dynamics after fasted mice were presented with food, due to the near complete, sustained silencing of these cells by caloric replenishment (Figure S5E–F). These experiments demonstrate that a rat predator threat has the capacity to lower AgRP activity in hungry animals, possibly serving to thwart feeding behavior under perilous circumstances.

PMd^{Cck} neurons respond to a rat predator and gate feeding behavior through AgRP inhibition

We next sought to identify brain regions activated by a rat predator via **T**argeted **R**ecombination in **A**ctive **P**opulations (TRAP)[46] that could potentially influence AgRP-evoked food intake, with a focus on the hypothalamic defensive network[36–38]. While we detected little to no Fos-induced tdTomato signal in the PMd in control animals, we

observed a striking increase in fluorescence in this region after rat presentation (Figure S6A).[16,36] Within the PMd is a large subset of excitatory neurons marked by the expression of cholecystokinin (Cck) that have recently been shown to respond to acute threat[39]. Conditional or viral directed expression of tdTomato/mCherry to PMd^{Cck} neurons (Figure 5A) revealed a high level of Cck+/Fos+ overlap specific to rat predator exposure (Figure 5B, S6B). We observed robust and sustained activation of PMd^{Cck} population activity during the introduction of a rat predator that has previously been linked to escape behavior (Figure S6C–E)[16]. Aligned with the notion that these cells encode danger, we found that PMd^{Cck} network dynamics were rapidly inhibited upon the first bite of food, when perceived threat/escape is low.

Unlike AgRP neurons, PMd^{Cck} activity was independent of hunger state as Fos levels were comparable between fed and fasted conditions (Figure S6F) and PMd^{Cck} calcium activity was not durably suppressed to food presentation compared to a non-food object (Figure S6C,G–H). Concordantly, acute silencing of PMd^{Cck} neurons, via bilateral transduction of the inhibitory DREADD actuator hM4Di (Figure 5C), failed to alter homecage food intake (Figure S6I). To determine if this was perturbation was context-specific, feeding was assessed in fasted mice in the presence of a rat predator. Suppression of PMd^{Cck} activity (via Clozapine-N-oxide, CNO) increased both food intake (Figure 5D) and time spent in the threat quadrant, housing the FED, nearest the rat predator, (Figure 5E) compared to the same animals without cell inhibition (saline). Importantly, control mice without DREADD expression exhibited no changes in feeding behavior following saline versus CNO injections (Figure S6J). These manipulations demonstrate a key role for PMd^{Cck} neurons in orchestrating the response to threat and gating feeding behavior.

To examine the sufficiency of these cells to diminish feeding, channelrhodopsin-2 (ChR2) was targeted to PMd^{Cck} neurons and behavior was assessed in a closed-loop optogenetic arena, whereby fasted mice received stimulation when they left the safe zone to forage for food (Figure 5F). PMd^{Cck} photoactivation reduced food intake and time spent in the FED zone and increased the latency to retrieve the first pellet and time spent in the safe zone compared to the same mice without light stimulation (Figure 5G–H, S6K–L). The majority of pellets procured and ingested in the no stimulation condition occurred with an IPI of 30 seconds or less (70.2%) with only a small fraction of pellets retrieved with an IPI of 60 seconds or greater (20.2%) (Figure 5I). However, PMd^{Cck} stimulation perturbed this pattern with mice consuming a higher number of pellets with an IPI of 60 seconds or greater (51.9%) than an IPI of 30 seconds or less (46.3%) (Figure 5I). Critically, control mice harboring no ChR2 expression displayed no changes in food intake or time spent in the stimulation zone in this paradigm (Figure S6M–N). This implies that PMd^{Cck} activation is capable of suppressing food-seeking and intake in hungry mice by mimicking the normal activity evoked by predator threat.

Since rat exposure acutely inhibited AgRP activity, we hypothesized PMd^{Cck} communication to AgRP neurons was a mechanism behind this hypophagic response. PMd^{Cck} neurons are excitatory[16,47], so we predicted this signaling would be indirect. Supporting this notion, anterograde mapping of PMd^{Cck} projections revealed no terminals to the ARC (Figure S7A) and ChR2-assisted circuit mapping failed to detect PMd^{Cck} light-

evoked post-synaptic currents[48] in AgRP neurons (Figure S7B). To assess a polysynaptic connection *in vivo*, we simultaneously transduced PMd^{Cck} and AgRP/NPY cells with stimulatory hM3Dq DREADD and GCaMP, respectively (Figure 6A). Due to the close proximity of the ARC and PMd (Figure S7C), we used a combination of Cre and FlpO reagents to eliminate viral cross contamination. Rat presentation inhibited AgRP/NPY activity in these *Npy*-ires2-FlpO animals, which was further reduced with food exposure, comparable to our prior observations using *AgRP*-ires-Cre mice (Figure S7D; Figure 4F–H). While control saline injections had no effect on AgRP/NPY responses, CNO-initiated PMd^{Cck} activation robustly and durably suppressed AgRP/NPY population dynamics (Figure 6B–D). Supporting the view that PMd^{Cck} stimulation specifically simulates threat exposure, rat predator presentation following CNO administration failed to further suppress AgRP/NPY activity, until food introduction (Figure 6E–F).

Redundancy among neural circuits underlying survival behaviors ensure appropriate outcomes are safeguarded if one specific pathway goes awry[28,49]. Predator exposure induced neural activity in several brain regions including the PMd (Figure S1). While silencing PMd^{Cck} activity increased food consumption under threat (Figure 5E), the effect was partial, implying the involvement of parallel networks acting to limit food-seeking under duress. To directly establish the necessity of PMd^{Cck} signaling for the threat-induced suppression of AgRP/NPY activity, we concurrently targeted PMd^{Cck} and AgRP/NPY cells with inhibitory hM4Di DREADD and GCaMP, respectively (Figure 6G). Unlike activation experiments, acute silencing of PMd^{Cck} neurons had no effect on AgRP/NPY population dynamics (Figure 6H, Figure S7E). Moreover, PMd^{Cck} inhibition failed to alter the rat predator-evoked suppression of AgRP/NPY activity (Figure 6H–I), suggesting alternative pathways are in place to prioritize self-preservation over food-seeking. Notably, CNO injections had no effect on AgRP/NPY population dynamics in non-DREADD-expressing control mice (Figure S7F–G). This finding uncovers a critical transmission between predator-responding PMd^{Cck} neurons and hunger-signaling AgRP neurons that act to impede feeding under hazardous conditions.

Feeding behavior under threat is scalable by internal state and mediated by AgRP neurons

Despite the need for safety, foraging is required for survival with longer periods of food deprivation driving a stronger motivation to pursue caloric replenishment. We found that a 48 hour fast significantly exacerbated food intake in both the empty cage and rat predator conditions compared to both sated and mice fasted overnight (Figure 7A–B). Notably, the rat stimulus suppressed feeding across all fasted states (Figure 7B). These experiments demonstrate an oscillating relationship between self-preservation and food seeking that is flexible and influenced by internal milieu. We next investigated the contribution of AgRP neurons in modulating feeding behavior in an ethologically-relevant context where a real-time cost-benefit decision must be made.

Chemogenetic inhibition of AgRP neurons decreased food intake in hungry mice in the empty cage condition as previously described (Figure 7C–D).[29] While rat predator exposure curtailed feeding in the control saline condition (Figure 7D), the residual food consumption that remained was further blunted with AgRP silencing (Figure 7D). Control mice without

DREADD expression exhibited comparable food intake in the saline versus CNO conditions but demonstrated reduced consumption in the rat predator versus empty cage context (Figure S8A). Although imperative for food odor attraction[50], NPY release from AgRP neurons is an unlikely contributor to food procurement/consumption during predator exposure, as NPY knockout animals displayed comparable levels of food intake as controls (Figure S8B). This suggests that AgRP neural activity is required, independent of NPY release, for the limited food eaten under threat.

Acute activation of AgRP neurons has been shown to promote food intake in calorically replete mice[27–29,51]. To test this under the duress of predation, we selectively targeted ChR2 to AgRP cells (Figure 7E). The same animals were tested in four discrete states 1) sated, 2) fasted overnight, 3) sated with concurrent AgRP photostimulation (sated$^{AgRP\ CS}$) and 4) sated with pre- AgRP photostimulation (sated$^{AgRP\ PS}$) in both the empty cage and rat predator conditions. In the empty cage condition, fasted mice ate significantly more than they did in the sated state, which was recapitulated in both the sated$^{AgRP\ CS}$ and sated$^{AgRP\ PS}$ states (Figure 7F; Figure S8C). This was due to a shorter latency to commence feeding (Figure 7G) and higher rate of intake (Figure 7H). IPI analysis revealed that the majority of all pellets consumed in the empty cage condition were done so with an IPI of <30 seconds (fasted 71.2%; sated$^{AgRP\ CS}$ 79.8%; sated$^{AgRP\ PS}$ 69.0%) with only a subset eaten with an IPI of >60 seconds (fasted 19.2%; sated$^{AgRP\ CS}$ 18.0%; sated$^{AgRP\ PS}$ 22.7%) (Figure 8I–L). Concordantly, these groups displayed elevated time spent in the FED Zone (Figure S8D). Rat exposure significantly suppressed food intake irrespective of state (Figure 7F) as animals moved toward higher occupancy of the Safe Zone (Figure S8E). However, mice in the fasted state still exhibited higher food intake (Figure 7F), shorter latency to procure the first pellet (Figure 7G) and a greater rate of feeding (Figure 7H) compared to the sated state in the presence of a rat predator, an effect that was mimicked via AgRP photoactivation. Rat exposure shifted the microstructure of feeding unidirectionally in all groups of mice as IPI's of <30 seconds and >60 seconds were decreased and increased, respectively, compared to the empty cage condition (Figure 7I–L). Animals in the fasted (Figure 7J) and sated$^{AgRP\ PS}$ (Figure 7L) states consumed a higher percentage of their pellets with an IPI of >60 seconds than <30 seconds. However, mice in the sated$^{AgRP\ CS}$ state continued to eat a larger proportion of their pellets with an IPI of <30 seconds (Figure 7K) likely due to the non-physiological nature of continuous AgRP stimulation in the presence of food[31,33,34].

To investigate the downstream targets of AgRP neurons that enable feeding behavior under threat, we again targeted ChR2 to AgRP cells and implanted optical fibers over terminal regions that spur eating (Figure 7M; Figure S8F). Photoactivation of AgRP axonal fields to the BNST, LH, PVH and PVT escalated food intake in the empty cage condition compared to no photostimulation (Figure 7N). However, only AgRP terminal activation in the BNST and LH was sufficient to drive feeding to a higher degree than the no stimulation control during rat exposure (Figure 7N) suggesting specificity for these pathways at the intersection of food-seeking and threat avoidance. All groups of photostimulated mice, independent of axonal field, exhibited diminished food intake in the presence of a rat compared to the empty cage condition (Figure 7N). Importantly, blue light did not affect feeding behavior in non-harboring ChR2 transgenic *AgRP*ires-Cre mice in both empty cage and predator

contexts (Figure S8G). Collectively, these studies demonstrate feeding behavior under threat is scalable by internal state and mediated by AgRP neural signaling downstream to the BNST and LH.

Discussion

Behavioral underpinnings of a risk-reward relationship

By designing an assay to study motivational conflict, we explored the behavioral relationship between two discrete need states: self-preservation in the face of an imminent threat and food procurement under caloric deficiency. This interaction embodies ethologically-relevant choice behavior made by prey species during natural food-seeking. While different threat stimuli often lead to variable responses[52], we report that rat predator exposure rapidly and robustly induced physiological, behavioral, and neuronal changes in mice signifying elevated levels of fear, anxiety-like behavior and stress. This predator context manifested attenuated quantitative and qualitative feeding behavior in hungry mice that failed to habituate or acclimate over repeated exposures.

Animals live in complex environments where predation risk and food availability/necessity change over time and consequently need to adapt their behavior to maximize fitness. Supporting the theoretical predation risk allocation hypothesis[5], we demonstrated that animals vacillate allocation efforts based on the intensity and probability of a predatory attack and current degrees of energy stores. While food-seeking and consumption remained sparse in the presence of a predator, strategies rapidly transformed when threat levels were reduced. Mice were more likely to retrieve pellets when the distance between the food source and predator grew larger and this reached baseline feeding levels after the rat was removed from the chamber entirely, demonstrating real-time decision-making that maximizes benefit when cost is low. Further lending support to this central tenet, we found that diminishing one arm of the conflict tips the scales toward the most beneficial outcome. While hungry mice tasked with procuring food from the threat zone were constantly switching between foraging and security, the same hungry animals exclusively occupied the safety zone when the food source was located there. Moreover, sated mice exhibited minimal food-seeking to the threat zone, opting to spend nearly all their time in the safety zone. These studies implicate that mice quickly estimate risk versus reward, amplifying and tempering food-seeking behavior based on receding and rising threat levels, respectively.

Predator exposure mimicked by PMd^{Cck} activation suppresses feeding and AgRP population dynamics

Paradigm-shifting studies uncovered that the sensory detection and/or anticipation of food rapidly inhibits AgRP neural activity, and the durability of this suppression is contingent on caloric consumption[31–35,53]. These experiments concluded that AgRP dynamics were specifically tuned toward future feeding events. We speculated that competing motivational drives, such as self-preservation under predator duress, could attenuate food intake by dampening AgRP activity. Indeed, we found that rat exposure promptly and persistently inhibited AgRP activity irrespective of food cues. This suggests that AgRP neurons act as a site of convergence integrating external cues such as the presence of a predator and

internal state to prioritize realtime needs and behavioral output. Sensory cues both directly and indirectly tied with food including those triggered by the presence of a predator can inform the animal about the status of a future feeding bout. Thus, it is plausible that an impending threat dampens AgRP activity to prioritize safety over food-seeking. This would suggest that contexts of intense stress and/or danger associated with hypophagia are at least in part a direct consequence of AgRP suppression. While individual AgRP neurons exhibit homogenous calcium response properties to food presentation[31], it is unknown whether a similar inhibitory profile would be observed during a predator encounter. Future studies employing microendoscopic imaging will help establish whether all or a subset of AgRP neurons respond to a predator threat as well as their putative overlap in dynamics with the same cells that respond to food.

Predator-induced Fos-Trapping navigated us to the PMd, part of the hypothalamic defense area[14–16,36–39], where a large proportion of responsive cells were marked by Cck. Despite not being endogenously coordinated by energy balance, acute PMd^{Cck} silencing gated feeding behavior in a context-specific manner, escalating food intake during rat exposure. This result likely occurs due to a decrease in escape behaviors[39]. Notably, these mice still displayed low levels of food intake in the presence of a predator suggesting parallel, redundant networks function to broadcast potential threat. Supporting this view, we found AgRP neurons are still suppressed in response to a rat predator during PMd^{Cck} neuronal inhibition. In contrast, PMd^{Cck} neural activation blunted feeding in hungry mice in the absence of danger, presumably through the encoding of a visceral threat. Like predator presentation, artificial PMd^{Cck} stimulation rapidly and durably inhibited AgRP population activity, via polysynaptic transmission. The two main outputs of the PMd are the PAG and anteromedial ventral thalamic nucleus (amv), which may in turn relay information to the ARC[54]. The nature of this communication could be direct, as monosynaptic rabies tracing implicates AgRP neurons receive efferents from the PAG or indirect via thalamic or midbrain signaling to the hypothalamus[55,56]. One potential route may be through upstream leptin receptor-expressing (Lepr) neurons of the dorsal medial hypothalamus (DMH) that respond to sensory cues and guide learning via dense inhibitory inputs to AgRP neurons[57,58]. Further studies are required to tease apart the nodes of communication linking these two subsets of cells.

Food-seeking under threat is governed by ARC^{AgRP} communication to the BNST and LH

Despite the dangers of food-seeking, prey species are often forced to procure the calories required for growth and propagation. This drive to forage scales with length of caloric deprivation[59]. While predator exposure suppressed AgRP activity, the magnitude of this inhibition was only partial compared to food presentation. Thus, this remaining AgRP activity may be involved in the residual feeding behavior observed under predator threat. Reinforcing this notion, AgRP silencing further reduced, while activation promoted, food intake in hungry and sated mice, respectively, during rat exposure. Interestingly, while both concurrent and pre-AgRP stimulation in sated mice drive quantitative food intake comparable to the fasted condition, only pre-AgRP photoactivation accurately reflects the qualitative feeding patterns seen in the fasted state. This is likely a consequence of the endogenous ARC^{AgRP} activity during food presentation[31,33,34]. Priming AgRP activity

in calorically replete animals communicates hunger but this artificial photostimulation is inhibited by food. The ensuing feeding following pre-AgRP activation is dependent on NPY[51]. Concurrent AgRP stimulation artificially locks animals into a state that fails to mimic physiological AgRP response properties to food[60,61].

Previous reports pinpointed a series of parallel, AgRP forebrain feeding circuits to the BNST, PVH, LH, PVT, MeA and medial preoptic area (MPOA)[28,30,62–64]. While each of these projections support food intake in an acclimated homecage where choice is limited, we hypothesized that discrete AgRP signaling networks were dedicated toward orchestrating feeding behavior during specific contexts. For instance, only selective stimulation of AgRP→PBN or AgRP→PVT axons blocks the behavioral response to inflammatory pain or promotes food odor attraction, respectively[50,65]. We demonstrated specific inhibitory AgRP projections to the BNST and/or LH were permissive to stimulate feeding behavior in the presence of a rat predator, while other orexigenic pathways were not. This suggests that hunger, encoded at the level of AgRP neurons, acts to dampen signals arising from a predator exposure in the BNST and/or LH ultimately enabling foraging and food consummation. While a number of studies have described cells in these regions that respond to threat or promote feeding[66–73], future experiments will be needed to address the specific molecular/behavioral identity and function of these downstream circuits, including whether perturbation of AgRP neurons influences PMd^{Cck} activity responses to predation risk.

Survival-based circuits are often studied in isolation giving a sense that activity drives behavior in direct and deceptively simple ways. In reality, multiple, redundant networks communicate across regions, constantly changing constraints and shaping attractor landscapes through a massive set of interlocking dynamical systems with a common purpose of optimizing behavior. Here, we employed a competition assay to explore the reciprocal influence and central mechanisms through which hunger and self-preservation impact one another to promote appropriate behavior on a moment-to-moment basis.

STAR METHODS

RESOURCE AVAILABILITY

Lead Contact—Further information and requests for resources should be directed to and will be fulfilled by the lead contact, Michael Krashes (michael.krashes@nih.gov).

Materials availability—This study did not generate new unique reagents.

Data and code availability—All data reported in this paper will be shared by the lead contact upon request.

All original code has been deposited at https://github.com/earnestt1234/FED3_Viz

Experimental Model and Study Participant Details

Mice: All animal care and experimental procedures were approved by the National Institute of Health Animal Care and Use Committee. Mice were kept under controlled conditions (22–24°C, with a light/dark cycle of 12 hours, starting at 6am). Standard chow

(Teklad F6 Rodent Diet 8664; 4.05 kcal g^{-1}, 3.3 kcal g^{-1} metabolizable energy, 12.5% kcal from fat; Harlan Teklad) and water were available *ad libitum*, unless otherwise stated. For all behavioral studies male and female mice between 5–18 weeks were singly-housed until the start of the experiments. We used the following mouse lines: *C57BL/6* (C57BL/6JRj; 000664; Jackson Laboratory; Bar Harbor, ME, USA), *Agrp-ires-Cre* mice (Agrp$^{tm1(cre)Lowl}$/J; 012899; Jackson Laboratory; Bar Harbor, ME, USA), *NPY-hrGFP* (*B6.FVB-Tg(Npy-hrGFP)1Lowl/J;* 006417; Jackson Laboratory; Bar Harbor, ME, USA), *Cck-ires-cre* (Cck$^{tm1.1(cre)Zjh}$/J; 012706; Jackson Laboratory; Bar Harbor, ME, USA), *Npy-ires2-FlpO* (Npy$^{tm1.1(flpo)Hze}$/J; 030211; Jackson Laboratory; Bar Harbor, ME, USA), *Fos^{2AiCreER}* (Fos$^{tm2.1(icre/ERT2)Luo}$/J; 030323; Jackson Laboratory; Bar Harbor, ME, USA) and *Crh-ires-Cre* (Krashes et al., 2014. Gift from Dr. Bradford Lowell), *NPY KO* (129S-Npy^{tm1Rpa}/J; 004545; Jackson Laboratory; Bar Harbor, ME, USA), *Ai14* (B6;129S6-Gt(ROSA)26Sor$^{tm14(CAG-tdTomato)Hze}$/J; 007908; Jackson Laboratory; Bar Harbor, ME, USA).

Rats: All animal care and experimental procedures were approved by the National Institute of Health Animal Care and Use Committee. Mice were kept under controlled conditions (22–24°C, with a light/dark cycle of 12 hours, starting at 6am). Standard chow (Teklad F6 Rodent Diet 8664; 4.05 kcal g^{-1}, 3.3 kcal g^{-1} metabolizable energy, 12.5% kcal from fat; Harlan Teklad) and water were available *ad libitum*, unless otherwise stated. Male Long Evans Rats (006; Charles River) were singly-housed and never handled to maintain their aggressive behaviors towards the mice.

Method Details

Conflict behavioral assay: The two-chambered apparatus measured 61×31×40cm with a perforated partition separating the the cage into two chambers (25×31×40 for the mice chamber; 36×31×40 for the stimulus side). The perforated wall does not restrict contact but prevents attack/physical harm. An automated pellet-dispenser, or Feeding Experimentation Device (FED3)[19,74], abutting the perforated wall, dispensed individual 20 mg grain pellets (TestDiet). On the opposite corner of the feeding device, a vertical opaque wall was placed to create a safe zone for the mice to hide behind. Mice were acclimated to experimental cages and the automated feeding device for 24 hours prior to experiments. Animals that didn't consume pellets from the pellet-dispenser were not used before the start of the experiment. Ad libitum water is always provided. Cumulative pellets consumed, pellets consumed per 200 seconds, inter-pellet interval and meal analysis were calculated using FEDviz software[19](https://github.com/earnestt1234/FED3_Viz). Meals were defined as a minimum of 3 pellets eaten within 1 min of each other. Pellets taken from the FED were automatically registered in the software and were verified via video to ensure pellet consumption. All trials were recorded on video using EthoVision XT 16.

Mice were fasted overnight (~16 hours) to increase their motivation to seek and eat food and tested during the day. All experiments were performed in a randomized, crossover design. All experiments were performed under low light conditions except for the experiment conducted in total darkness. Animals were moved to the specialized cage for a 20 minute Acclimation Phase with the FED off. Mice were then exposed to four possible stimuli 1)

empty cage, 2) stuffed rat, 3) a filter paper infused with 10 μl of 2,3,5-trimethyl-3-thiazoline (TMT), or 4) a rat predator during a 20 minute Trial phase with the FED on. This was followed by a 20 min Post phase when the various stimuli were removed from the adjacent cage with the FED on (Figure S2A). In the repeated exposure experiments, each animal went through this procedure to the various stimuli across four separate trials. In the conflict elimination experiments, mice were also tested in the sated condition and in a context where the FED was repositioned from the Threat Zone abutting the perforated wall to the Safety Zone behind the hide wall. The rats' spatial position (snout) in the adjacent cage was scored each time a mouse retrieved a food pellet. In the near/far experiments, the rat was repositioned to 12×14×40 area either nearest or farthest away from the FED. All chemogenetic experimental mice were handled and injected with saline ip daily for at least 7 days prior to the experiment to minimize stress of injection. Injections of saline or CNO (3mg/kg) were administered 60 minutes prior to the start of the experiment. All optogenetic and photometry mice were handled and hooked up to a patchcord daily for at least 7 days prior to the experiment to minimize stress.

Stereotaxic surgery and viral injections: Stereotaxic injections were performed as previously described[75]. Six weeks old mice were anaesthetized with 5% isoflurane and placed in a stereotaxic apparatus (Stoelting Just for Mice) where anesthesia was maintained with 2% isoflurane. A craniotomy was performed, and viral vectors were injected using a glass pipette with a tip diameter of 20–40 μm attached to air pressure system. A micromanipulator (Grass Technologies, Model S48 Stimulator) was used to control injection speed at 25 nl min^{-1} and the pipette was withdrawn 5 min after injection. After surgery, mice were injected subcutaneously intraperitoneally with meloxicam (0.5 mg per kg), rehydrated with saline (0.9% NaCl) ip and monitored until recovery. The following coordinates relative to bregma were used for ARC (AP + 1.5, ML ± 0.25, DV −5.70, PMd (AP −2.46, ML ± 0.5, DV −5.35) and PVH (AP −0.72, ML ± 0.22, DV −4.70). For chemogenetic experiments, mice were injected bilaterally with AAV9-hSyn-DIO-hM3dq-mcherry (1.1×10^{13} vg/ml) or AAV9-hsyn-DIO-hM4dimcherry (1.1×10^{12} vg/ml) in PMd (50nl). Unilateral injections of AAV9-CAG-Flex-ChR2-tdTomato (1.1×10^{13} vg/ml) or pAAV-CAG-DIO-ChR2(H134R)-eYFP (1.1×10^{13} vg/ml) in the ARC (200nl) or PMd (50nl) were used for optogenetic studies. For fiber photometry experiments, AAV1-CAG-FLEX-GCaMP6s-WPRE-SV40 (1.1×10^{13} vg/ml), AAV1-CAG-FLEX-X-jG-GCaMP7s-WPRE (7×10^{12} vg/ml) or AAV8-EF1a-fDIO-GCaMP6s (1.1×10^{13} vg/ml) was unilaterally injected into the ARC (300nl) PVH (50 nL) or the PMd (50nl).

Optic Fiber Implantation: For optical experiments, fibers (200 μm diameter core; BFH37–200 Multimode; NA 0.37; Thor Labs) were implanted unilaterally over the ARC (bregma: AP: −1.50 mm, ML: −/+ 0.25 mm, DV: −5.55 mm), the PMd (bregma: AP: −2.46 mm, ML: −/+ 0.5 mm, DV: −5.20 mm), the aBNST (bregma: AP: +0.4 mm, ML: −/+ 0.5 mm, DV: −4.12 mm), the LH (bregma: AP: −1.32 mm, ML: −/+ 1.00 mm, DV: −4.30 mm), the PVH (bregma: AP: −0.72 mm, ML: −/+ 0.25 mm, DV: −4.35 mm) and PVT (bregma: AP: −1.1 mm, ML: −/+ 0.00 mm, DV: −2.60 mm). Fibers were fixed to the skull using C&B Metabond Quick Cement and dental acrylic and mice were allowed 2 weeks for recovery.

Photostimulation protocol: Fiber optic cables (1 m long, 200 mm diameter; Doric Lenses) coupled to a laser via a fiber-optic rotary joint (Doric Lenses), were attached to the fiber optic cannulae with zirconia sleeves (Doric Lenses). For photostimulation AgRP-positive neurons in the ARC and their terminal fields, light pulse trains (20HZ; 2 sec on, 2 sec off; 473nm from Laserglow laser technologies) were programmed using a waveform generator (PCGU100; Valleman Instruments) for continuous photostimulation during all trials. The light power exiting the fiber optic cable was 10–12 mW. For photostimulation of Cck-positive neurons in the PMd, pulse trains (20HZ; 2 sec on, 2 sec off; 473nm from Laserglow laser technologies) were custom programmed with Arduino electronics and continued for as long as the mouse remained on the side of the chamber paired with photostimulation. All optogenetic mice were tethered to the patchcord and acclimated during the Acclimation Phase where no blue light stimulation except for the case of priming AgRP neurons. For PMd^{Cck} photostimulation a closed loop system was used where pulse trains continued for as long as the mouse remained in the three quadrants of the chamber paired with photostimulation. Only the safe zone quadrant behind the hide wall was unpaired with photoactivation.

Screening protocol for AgRP photostimulation-evoked feeding: Screening for all *Agrp-IRES-Cre* mice with optical fibers implanted over the ARC or over AgRP terminals (aBNST, PVH, LH and PVT) was conducted in the homecage at the beginning of the light cycle when food intake is normally low. Sated animals were tethered to the fiber and acclimated for 20 minutes without food. After the acclimatization period, mice were given *ad-libitum* access to standard chow for a 40-minute with photostimulation (as described). Only mice that consumed >0.30g of standard chow during the photostimulation period were selected for the experiments.

In vivo fiber photometry: Unilateral optic-fiber cannulas (fiber: core=400μm; NA=0.48; M3 thread titanium receptacle; Doric Lenses Inc) were implanted in the ARC (bregma: AP: −1.5 mm, ML: −/+ 0.25 mm, DV: −4.70 mm), the PVH (bregma: AP: −0.72 mm, ML: −/+ 0.22 mm, DV: −4.40 mm) or the PMd (bregma: AP: −2.54 mm, ML: −/+ 0.5 mm, DV: −5.20 mm) of each experimental mouse. Behavioral testing started 4 weeks later to allow for viral expression and recovery from surgery. Mice were then allowed to adapt to the experimental cages and tethered patch cord for at least 2 days prior to experiments (core 400 uM; NA 0.53; M3 connector; Doric Lenses Inc). Continuous ~20 uW blue LED at 465 nm served as a light source driven by a multichannel hub (Thorlabs), modulated at 211hz and 511hz respectively, and delivered to a filtered minicube (FMC5, Doric Lenses) before connecting through optic fibers to a rotary joint (FRJ 1 3 1, Doric Lenses) to allow for movement. GCaMP calcium GFP signals were collected through the same fibers via a dichroic mirror of the minicube into a femtowatt silicon photoreceiver (2151, Newport). Signals were then demodulated, amplified, and collected through a lock-in amplifier (RZ5P, Tucker-Davis Technologies). Data was collected through the software Synapse (TDT), exported via Browser (TDT), and analyzed in Microsoft Excel.

PVH^{Crh} photometry in the presence of a predator: *Crh*-ires-Cre mice were placed in the specialized cage for a 20 minute acclimatization period. A stuffed rat or a rat predator was

presented for 10 minutes. Lastly, the stuffed rat or a rat predator was removed, and activity was recorded for 10 more minutes

AgRP photometry in the presence of a predator: *AgRP*-ires-cre mice were fasted overnight and placed in the specialized cage the next day, for a 20 minute acclimatization period with the FED off. A stuffed rat or a rat predator was presented for 10 minutes with the FED off. During the next 10 minutes the FED was turned on in the presence of the stuffed rat or a rat predator. Lastly, the stuffed rat or a rat predator was removed, and activity was recorded for 10 more minutes with FED still on. To test whether the rat-evoked suppression of AgRP activity was reversible, fasted mice were presented with a rat predator for either 2 or 10 minutes at which point the rat was extracted. After 20 minutes, food was presented to the mice. To test whether a rat predator stimulus could further suppress AgRP activity after food presentation, fasted mice were presented with food for 10 minutes followed by rat predator introduction.

PMd^{Cck} photometry: *Cck*-ires-Cre mice expressing GCaMP6s were fasted overnight and placed in the specialized cage the next day, for a 20 minute acclimatization period. On different days, either a stuffed rat, rat predator, food, or nonfood object (15 mL Falcon tube cap) was presented for 5 minutes.

NPY photometry and PMd^{Cck} neuron manipulation: For activation experiments, *Npy*-ires2-FlpO mice crossed with *Cck*-ires-cre mice expressing hM3dq in the PMd and GCaMP6s in the ARC, respectively, were fasted overnight and placed in the specialized cage the next day, without access of food, for a 20 minute acclimatization period. Following a 10 minute baseline recording, mice received an injection with either CNO (1 mg/kg) or saline in a randomized crossover design. After 20 minutes post-injection, food was given and NPY neuronal activity was recorded for 10 more minutes. To determine whether a rat predator could further suppress AgRP activity following PMd^{Cck} activation, *Npy*-ires2-FlpO; *Cck*-ires-cre mice expressing hM3dq in the PMd and GCaMP6s in the ARC, respectively, were fasted overnight and placed in the specialized cage the next day, without access of food, for a 20 minute acclimatization period. Following a 10 minute baseline recording, mice received an injection of CNO (1 mg/kg) and after 20 minutes a rat predator was introduced into the adjacent cage. Following another 10 minutes, food was presented into the cage.

For inhibition experiments, *Npy*-ires2-FlpO mice crossed with *Cck*-ires-cre mice expressing hM4di in the PMd and GCaMP6s in the ARC, respectively, were fasted overnight and placed in the specialized cage the next day, without access of food, for a 20 minute acclimatization period. Following a 10 minute baseline recording, mice received an injection with either CNO (3 mg/kg) or saline in a randomized crossover design. After 20 minutes post-injection, a rat predator was introduced in the adjacent cage. After another 10 minutes food was given and NPY neuronal activity was recorded for 10 more minutes. Critically, control *Npy*-ires2-FlpO; *Cck*-ires-cre mice expressing a fluorophore in the PMd and GCaMP6s in the ARC demonstrated no response to CNO.

Photometry analysis: dF/F were calculated using the formula: (100 * (F-F0)/F0) where F is the fluorescent ratio value of a given frame and F0 was defined as the mean F value

during the 5 minutes prior the introduction of the stuffed rat/rat predator. Normalized dF/F were calculated by designating the food drop at −1 (last 5 minutes during the removal of the stuffed rat/rat predator or 25 minutes after saline/CNO i.p. injection) and the baseline (F0) at 0. Quantified responses to stuffed rat/rat predator or saline/CNO or CNO/Rat predator were measured as the mean normalized dF/F value during the last 5 minutes of recording after introducing the stimulus.

Telemetry: Mice were implanted with an intra-arterial pressure telemetry probe (model HD-X10, Data Sciences International, St Paul, MN) to collect blood pressure, heart rate, temperature, and activity in a freely moving mouse. Weeks after surgeries, animals were housed in a 45×30×20 cm cage for at least 7 days. 1 hour before the beginning of the recording, at onset of the light cycle, food, water, and nesting material were removed from the cage and a perforated wall was added to divide the cage in two. A 10-minute baseline recording was performed in sated mice before a stuffed rat was introduced into the cage for 10 minutes before being removed. Following another 10 minutes of recording in which the mouse was alone in the cage, a rat predator was presented to the animal. After 10 minutes, the rat predator was removed, and physiological recordings were recorded for an additional 10 minutes. Data were sampled at 1000 Hz, processed using a PhysioTel RPC-1 receiver, and collected with Ponemah v6.30 (Data Sciences International). 1 min averages were used for analysis. Physical activity is measured in arbitrary counts.

Electrophysiology: *Cck*-ires-Cre; *Npy*-hrGFP mice (6–12 weeks) received bilateral 50 nl injections of AAV1-Ef1a-DIO-ChR2-tdTomato in the PMd. Four to 6 weeks later, brain slices were obtained and stored at 30 °C in a heated, oxygenated chamber containing aCSF (in mmol/l) 124 NaCl, 4.4 KCl, 2 $CaCl_2$, 1.2 $MgSO_4$, 1 NaH_2PO_4, 10.0 glucose, and 26.0 sodium bicarbonate before being transferred to a submerged recording chamber maintained at 30 °C (Warner Instruments, Hamden, CT). Recording electrodes (3–5 MΩ) were pulled with a Flaming-Brown Micropipette Puller (Sutter Instruments, Novato, CA) using thin-walled borosilicate glass capillaries.

Light evoked inhibitory postsynaptic currents (IPSCs) were measured in voltage-clamp mode using electrodes filled with an intracellular recording solution containing (in mM): 135 Cs-methanesulfonate, 10 KCl, 10 HEPES, 1 $MgCl_2$, 0.2 EGTA, 4 Mg-ATP, 0.3 GTP, 20 phosphocreatine, 2 QX314. Npy GFP+ neurons were held at +10 mV to isolate GABAergic synaptic transmission and record spontaneous IPSCs within individual neurons. Tetrodotoxin (TTX, 500 nM) and 4-aminopyridine (4-AP, 100 μM) were included in the bath aCSF.

Corticosterone Assay, fecal output, and immobility assessment: All experiments were performed in ad libitum fed animals near the beginning of the light cycle. *C57BL/6J* mice were age- and weight-matched into their respective groups. *C57BL/6J* mice were housed in a 45×30×20 cm cage for at least 1 week to minimize stress. Prior to the introduction or either a stuffed rat or rat predator, nesting material and food was removed from the cage in addition the installation of a perforated wall. Both the number of fecal pellets and total time spent immobile was calculated after a 20 minute exposure in a crossover design. A separate cohort of male *C57BL/6J* mice were prepared in an identical manner. Two hours after the

introduction of either the stuffed rat or rat predator, mice were restrained, and tail vein blood collected. Corticosterone was measured by RIA (MP Biomedicals, Orangeburg, NY).

Fos Analyses: For predator Fos studies, *C57BL/6J*, *Npy*-hrGFP, *Cck*-ires-Cre; Ai14-*tdTomato*, and *Cck*-ires-Cre::hM4Di-mCherry animals were housed in a 45×30×20 cm cage for at least 1 week with ad libitum access to water, food and nesting materials. *Npy*-hrGFP mice were food-deprived for 24 hours. Early in the beginning of the light cycle, the food, the water, and the nesting material were removed from the cage and a perforated wall was added to divide the cage in two. Directly after, a stuffed rat or the rat predator was introduced into the empty side. 120 min later, the animals were euthanized with 7% chloral hydrate diluted in saline (350 mg/kg) for histological assay. To determine if PMd^{Cck} activity was regulated by appetite state, *Cck*-ires-Cre::hM4Di-mCherry were either food-deprived for 24 hours or provided *ad libitum* food in their homecage before euthanization process above. The mice were perfused and brains were sectioned as described below. Brain sections were processed for immunohistochemical detection of Fos, Fos and NPY-hrGFP or Fos and Cck::tdTomato/mCherry.

Brain tissue preparation and immunohistochemistry: Mice were perfused with fresh 4% paraformaldehyde (PFA). Subsequently, the brains were extracted and left in 4% PFA overnight, cryoprotected with 30% sucrose for 48h and cut in 50 μm free-floating sections using a Leica VT1200S vibratome. *Npy*-hrGFP, *Cck*-ires-Cre, *AgRP*-ires-Cre and C57BL/6J animals were socially isolated and handled daily for at least 1 week prior to Fos analyses. Brains were sectioned at 50 μm and incubated with primary antibody against Fos (ABE457, Millipore-Sigma, St-Louis, MO, USA, 1:1000) in PBS supplemented with 0.1% TritonX-100 and 5% NGS for 24h at 4°C. Sections were washed and incubated either in secondary antibody donkey anti-rabbit-AlexaFluor488 (**A32790**, Thermo Fisher Scientific, US) or in in secondary antibody donkey anti-rabbit-AlexaFluor594 (**A21207**, Thermo Fisher Scientific, US) diluted 1:1000 in PBS/0.1% TritonX-100 for 3h at room temperature. After several washes in PBS, sections were mounted in Vectashield mounting media (Vector labs). Brain sections were imaged on a Zeiss LSM 710 inverted confocal microscope (20x, NA = 0.8) and a digital slide scanner (VS200, Olympus, Japan) at 20 x magnification. Counting of Fos positive cells and colocalization was done using QuPath's positive cell detection plugin (https://qupath.github.io/). For each fluorescent image, regions of interest were drawn manually based on the regional boundaries from "The Mouse Brain in Stereotaxic Coordinates" by Franklin and Paxinos (2008).

Trap induction: *$Fos^{2A\text{-}iCreER}$* mice[46] were crossed with *Ai14* reporter mice. Mice were housed in a 45×30×20cm cage and were handled and injected with saline ip daily for at least 7 days prior to the experiment to minimize labeling due to handling and injections. On experimental day, a perforated wall was added to divide the cage in two and food, water and nesting materials were removed before a stuffed rat or rat predator was added. One hour after stimuli exposure, all mice received 10 mg/kg of 4-hydroxytamoxifen (4OHT, Sigma H6278) by ip injection. Four hours after ip injection, the stuffed rat or rat predator was removed from the cage. Two to three weeks after induction, mice were euthanized and perfused for histological analysis.

Drugs: 4-hydroxytamoxifen (4OHT, Sigma H6278) was dissolved in DMSO (100mM) and stored as single-use *aliquots* at −80°C until use. On the day of testing, the aliquot (25μl) was thawed, diluted in saline solution with 2% of Tween 80, for a final injectable solution containing 1mg/ml 4OHT, 1% Tween 80 and 2.5% DMSO in saline.

Quantification and Statistical Analyses: For comparisons between two groups, unpaired or paired two-tailed t tests were used. Repeated measures one-way or two-way analysis of variance (ANOVA) were applied for comparisons across groups or between groups over times. Significant tests were followed by a post-hoc multiple comparison analysis. Normality and equal variances were assumed. Pearson correlation coefficient was used to measure the linear correlation between data sets. Statistical analyses were done using Excel software and PRISM 8 software (GraphPad, San Diego, CA). All data are reported as mean ± standard error measurement.

Supplementary Material

Refer to Web version on PubMed Central for supplementary material.

Acknowledgments

We thank the NIDDK Mouse Metabolism Core and NHLBI Murine Phenotyping Core for their assistance with corticosterone measurements and telemetry surgeries, respectively. We thank all members of the Krashes lab for support and guidance. This research was funded and supported by the Intramural Research Program of the National Institutes of Health and the National Institute of Diabetes and Digestive and Kidney Diseases (DK075088 and DK075087–06 to M.J.K.), the Washington University Diabetes Research Center Pilot and Feasibility Grant (A.V.K.), the Washington University Nutrition Obesity Research Center (NORC) Pilot and Feasibility Program (A.V.K.), and the Center on Compulsive Behaviors Grant (I.A.S.).

Inclusion and diversity

We support inclusive, diverse, and equitable conduct of research.

References

1. Flavell SW, Gogolla N, Lovett-Barron M, and Zelikowsky M (2022). The emergence and influence of internal states. Neuron 110, 2545–2570. 10.1016/j.neuron.2022.04.030. [PubMed: 35643077]
2. Grillner S, Hellgren J, Ménard A, Saitoh K, and Wikström MA (2005). Mechanisms for selection of basic motor programs--roles for the striatum and pallidum. Trends Neurosci. 28, 364–370. 10.1016/j.tins.2005.05.004. [PubMed: 15935487]
3. Toates FM (1981). The control of ingestive behaviour by internal and external stimuli--a theoretical review. Appetite 2, 35–50. 10.1016/s0195-6663(81)80035-9. [PubMed: 7039503]
4. Levine DN (2007). Sherrington's "The Integrative action of the nervous system": a centennial appraisal. J. Neurol. Sci 253, 1–6. 10.1016/j.jns.2006.12.002. [PubMed: 17223135]
5. Lima SL, and Bednekoff PA (1999). Temporal Variation in Danger Drives Antipredator Behavior: The Predation Risk Allocation Hypothesis. Am. Nat 153, 649–659. 10.1086/303202. [PubMed: 29585647]
6. Amir A, Lee S-C, Headley DB, Herzallah MM, and Pare D (2015). Amygdala Signaling during Foraging in a Hazardous Environment. J. Neurosci. Off. J. Soc. Neurosci 35, 12994–13005. 10.1523/JNEUROSCI.0407-15.2015.
7. Dent CL, Isles AR, and Humby T (2014). Measuring risk-taking in mice: balancing the risk between seeking reward and danger. Eur. J. Neurosci 39, 520–530. 10.1111/ejn.12430. [PubMed: 24283296]

8. Franks B, Higgins ET, and Champagne FA (2012). Evidence for individual differences in regulatory focus in rats, Rattus norvegicus. J. Comp. Psychol. Wash. DC 1983 126, 347–354. 10.1037/a0027244.

9. Simon NW, Gilbert RJ, Mayse JD, Bizon JL, and Setlow B (2009). Balancing risk and reward: a rat model of risky decision making. Neuropsychopharmacol. Off. Publ. Am. Coll. Neuropsychopharmacol 34, 2208–2217. 10.1038/npp.2009.48.

10. Tye KM (2018). Neural Circuit Motifs in Valence Processing. Neuron 100, 436–452. 10.1016/j.neuron.2018.10.001. [PubMed: 30359607]

11. Xiong XR, Liang F, Zingg B, Ji X, Ibrahim LA, Tao HW, and Zhang LI (2015). Auditory cortex controls sound-driven innate defense behaviour through corticofugal projections to inferior colliculus. Nat. Commun 6, 7224. 10.1038/ncomms8224. [PubMed: 26068082]

12. Yilmaz M, and Meister M (2013). Rapid innate defensive responses of mice to looming visual stimuli. Curr. Biol. CB 23, 2011–2015. 10.1016/j.cub.2013.08.015. [PubMed: 24120636]

13. Blanchard DC, Griebel G, and Blanchard RJ (2003). Conditioning and residual emotionality effects of predator stimuli: some reflections on stress and emotion. Prog. Neuropsychopharmacol. Biol. Psychiatry 27, 1177–1185. 10.1016/j.pnpbp.2003.09.012. [PubMed: 14659473]

14. Cezario AF, Ribeiro-Barbosa ER, Baldo MVC, and Canteras NS (2008). Hypothalamic sites responding to predator threats--the role of the dorsal premammillary nucleus in unconditioned and conditioned antipredatory defensive behavior. Eur. J. Neurosci 28, 1003–1015. 10.1111/j.1460-9568.2008.06392.x. [PubMed: 18691328]

15. Silva BA, Mattucci C, Krzywkowski P, Murana E, Illarionova A, Grinevich V, Canteras NS, Ragozzino D, and Gross CT (2013). Independent hypothalamic circuits for social and predator fear. Nat. Neurosci 16, 1731–1733. 10.1038/nn.3573. [PubMed: 24212674]

16. Wang W, Schuette PJ, Nagai J, Tobias BC, Cuccovia V Reis FM, Ji S, de Lima MAX, LaVu MQ, Maesta-Pereira S, Chakerian M, et al. (2021). Coordination of escape and spatial navigation circuits orchestrates versatile flight from threats. Neuron 109, 1848–1860.e8. 10.1016/j.neuron.2021.03.033. [PubMed: 33861942]

17. Crawford M, and Masterson FA (1982). Species-specific defense reactions and avoidance learning. An evaluative review. Pavlov. J. Biol. Sci 17, 204–214. 10.1007/BF03001275.

18. Fanselow MS, Lester LS, and Helmstetter FJ (1988). Changes in feeding and foraging patterns as an antipredator defensive strategy: a laboratory simulation using aversive stimulation in a closed economy. J. Exp. Anal. Behav 50, 361–374. 10.1901/jeab.1988.50-361. [PubMed: 3209954]

19. Matikainen-Ankney BA, Earnest T, Ali M, Casey E, Wang JG, Sutton AK, Legaria AA, Barclay KM, Murdaugh LB, Norris MR, et al. (2021). An open-source device for measuring food intake and operant behavior in rodent home-cages. eLife 10, e66173. 10.7554/eLife.66173. [PubMed: 33779547]

20. Sutton AK, and Krashes MJ (2020). Integrating Hunger with Rival Motivations. Trends Endocrinol. Metab. TEM 31, 495–507. 10.1016/j.tem.2020.04.006. [PubMed: 32387196]

21. Swanson LW (2000). Cerebral hemisphere regulation of motivated behavior. Brain Res. 886, 113–164. 10.1016/s0006-8993(00)02905-x. [PubMed: 11119693]

22. Cowley MA, Smith RG, Diano S, Tschöp M, Pronchuk N, Grove KL, Strasburger CJ, Bidlingmaier M, Esterman M, Heiman ML, et al. (2003). The distribution and mechanism of action of ghrelin in the CNS demonstrates a novel hypothalamic circuit regulating energy homeostasis. Neuron 37, 649–661. 10.1016/s0896-6273(03)00063-1. [PubMed: 12597862]

23. Elias CF, Aschkenasi C, Lee C, Kelly J, Ahima RS, Bjorbaek C, Flier JS, Saper CB, and Elmquist JK (1999). Leptin differentially regulates NPY and POMC neurons projecting to the lateral hypothalamic area. Neuron 23, 775–786. 10.1016/s0896-6273(01)80035-0. [PubMed: 10482243]

24. Graham M, Shutter JR, Sarmiento U, Sarosi I, and Stark KL (1997). Overexpression of Agrt leads to obesity in transgenic mice. Nat. Genet 17, 273–274. 10.1038/ng1197-273. [PubMed: 9354787]

25. Ollmann MM, Wilson BD, Yang YK, Kerns JA, Chen Y, Gantz I, and Barsh GS (1997). Antagonism of central melanocortin receptors in vitro and in vivo by agouti-related protein. Science 278, 135–138. 10.1126/science.278.5335.135. [PubMed: 9311920]

26. Rossi M, Kim MS, Morgan DG, Small CJ, Edwards CM, Sunter D, Abusnana S, Goldstone AP, Russell SH, Stanley SA, et al. (1998). A C-terminal fragment of Agouti-related protein

increases feeding and antagonizes the effect of alpha-melanocyte stimulating hormone in vivo. Endocrinology 139, 4428–4431. 10.1210/endo.139.10.6332. [PubMed: 9751529]

27. Aponte Y, Atasoy D, and Sternson SM (2011). AGRP neurons are sufficient to orchestrate feeding behavior rapidly and without training. Nat. Neurosci 14, 351–355. 10.1038/nn.2739. [PubMed: 21209617]
28. Betley JN, Cao ZFH, Ritola KD, and Sternson SM (2013). Parallel, redundant circuit organization for homeostatic control of feeding behavior. Cell 155, 1337–1350. 10.1016/j.cell.2013.11.002. [PubMed: 24315102]
29. Krashes MJ, Koda S, Ye C, Rogan SC, Adams AC, Cusher DS, Maratos-Flier E, Roth BL, and Lowell BB (2011). Rapid, reversible activation of AgRP neurons drives feeding behavior in mice. J. Clin. Invest 121, 1424–1428. 10.1172/JCI46229. [PubMed: 21364278]
30. Padilla SL, Qiu J, Soden ME, Sanz E, Nestor CC, Barker FD, Quintana A, Zweifel LS, Rønnekleiv OK, Kelly MJ, et al. (2016). Agouti-related peptide neural circuits mediate adaptive behaviors in the starved state. Nat. Neurosci 19, 734–741. 10.1038/nn.4274. [PubMed: 27019015]
31. Betley JN, Xu S, Cao ZFH, Gong R, Magnus CJ, Yu Y, and Sternson SM (2015). Neurons for hunger and thirst transmit a negative-valence teaching signal. Nature 521, 180–185. 10.1038/nature14416. [PubMed: 25915020]
32. Beutler LR, Chen Y, Ahn JS, Lin Y-C, Essner RA, and Knight ZA (2017). Dynamics of GutBrain Communication Underlying Hunger. Neuron 96, 461–475.e5. 10.1016/j.neuron.2017.09.043. [PubMed: 29024666]
33. Chen Y, Lin Y-C, Kuo T-W, and Knight ZA (2015). Sensory detection of food rapidly modulates arcuate feeding circuits. Cell 160, 829–841. 10.1016/j.cell.2015.01.033. [PubMed: 25703096]
34. Mandelblat-Cerf Y, Ramesh RN, Burgess CR, Patella P, Yang Z, Lowell BB, and Andermann ML (2015). Arcuate hypothalamic AgRP and putative POMC neurons show opposite changes in spiking across multiple timescales. eLife 4. 10.7554/eLife.07122.
35. Su Z, Alhadeff AL, and Betley JN (2017). Nutritive, Post-ingestive Signals Are the Primary Regulators of AgRP Neuron Activity. Cell Rep. 21, 2724–2736. 10.1016/j.celrep.2017.11.036. [PubMed: 29212021]
36. Canteras NS, Chiavegatto S, Ribeiro do Valle LE, and Swanson LW (1997). Severe reduction of rat defensive behavior to a predator by discrete hypothalamic chemical lesions. Brain Res. Bull 44, 297–305. 10.1016/s0361-9230(97)00141-x. [PubMed: 9323445]
37. Fuchs SA, Edinger HM, and Siegel A (1985). The organization of the hypothalamic pathways mediating affective defense behavior in the cat. Brain Res. 330, 77–92. 10.1016/0006-8993(85)90009-5. [PubMed: 4039213]
38. Lammers JH, Kruk MR, Meelis W, and van der Poel AM (1988). Hypothalamic substrates for brain stimulation-induced patterns of locomotion and escape jumps in the rat. Brain Res. 449, 294– 310. 10.1016/0006-8993(88)91045-1. [PubMed: 3395850]
39. Wang W, Schuette PJ, La-Vu MQ, Torossian A, Tobias BC, Ceko M, Kragel PA, Reis FM, Ji S, Sehgal M, et al. (2021). Dorsal premammillary projection to periaqueductal gray controls escape vigor from innate and conditioned threats. eLife 10, e69178. 10.7554/eLife.69178. [PubMed: 34468312]
40. Deng H, Xiao X, and Wang Z (2016). Periaqueductal Gray Neuronal Activities Underlie Different Aspects of Defensive Behaviors. J. Neurosci. Off. J. Soc. Neurosci 36, 7580–7588. 10.1523/JNEUROSCI.4425-15.2016.
41. Evans DA, Stempel AV, Vale R, Ruehle S, Lefler Y, and Branco T (2018). A synaptic threshold mechanism for computing escape decisions. Nature 558, 590–594. 10.1038/s41586-018-0244-6. [PubMed: 29925954]
42. Gross CT, and Canteras NS (2012). The many paths to fear. Nat. Rev. Neurosci 13, 651–658. 10.1038/nrn3301. [PubMed: 22850830]
43. Kim JJ, Rison RA, and Fanselow MS (1993). Effects of amygdala, hippocampus, and periaqueductal gray lesions on short- and long-term contextual fear. Behav. Neurosci 107, 1093–1098. 10.1037//0735-7044.107.6.1093. [PubMed: 8136063]

44. Hahn TM, Breininger JF, Baskin DG, and Schwartz MW (1998). Coexpression of Agrp and NPY in fasting-activated hypothalamic neurons. Nat. Neurosci 1, 271–272. 10.1038/1082. [PubMed: 10195157]
45. van den Pol AN, Yao Y, Fu L-Y, Foo K, Huang H, Coppari R, Lowell BB, and Broberger C (2009). Neuromedin B and gastrin-releasing peptide excite arcuate nucleus neuropeptide Y neurons in a novel transgenic mouse expressing strong Renilla green fluorescent protein in NPY neurons. J. Neurosci. Off. J. Soc. Neurosci 29, 4622–4639. 10.1523/JNEUROSCI.3249-08.2009.
46. DeNardo LA, Liu CD, Allen WE, Adams EL, Friedmann D, Fu L, Guenthner CJ, TessierLavigne M, and Luo L (2019). Temporal evolution of cortical ensembles promoting remote memory retrieval. Nat. Neurosci 22, 460–469. 10.1038/s41593-018-0318-7. [PubMed: 30692687]
47. Mickelsen LE, Flynn WF, Springer K, Wilson L, Beltrami EJ, Bolisetty M, Robson P, and Jackson AC (2020). Cellular taxonomy and spatial organization of the murine ventral posterior hypothalamus. eLife 9, e58901. 10.7554/eLife.58901. [PubMed: 33119507]
48. Petreanu L, Huber D, Sobczyk A, and Svoboda K (2007). Channelrhodopsin-2-assisted circuit mapping of long-range callosal projections. Nat. Neurosci 10, 663–668. 10.1038/nn1891. [PubMed: 17435752]
49. Zimmerman CA, and Knight ZA (2020). Layers of signals that regulate appetite. Curr. Opin. Neurobiol 64, 79–88. 10.1016/j.conb.2020.03.007. [PubMed: 32311645]
50. Horio N, and Liberles SD (2021). Hunger enhances food-odour attraction through a neuropeptide Y spotlight. Nature 592, 262–266. 10.1038/s41586-021-03299-4. [PubMed: 33658716]
51. Chen Y, Essner RA, Kosar S, Miller OH, Lin Y-C, Mesgarzadeh S, and Knight ZA (2019). Sustained NPY signaling enables AgRP neurons to drive feeding. eLife 8, e46348. 10.7554/eLife.46348. [PubMed: 31033437]
52. Fendt M, and Endres T (2008). 2,3,5-Trimethyl-3-thiazoline (TMT), a component of fox odor - just repugnant or really fear-inducing? Neurosci. Biobehav. Rev 32, 1259–1266. 10.1016/j.neubiorev.2008.05.010. [PubMed: 18579206]
53. Mazzone CM, Liang-Guallpa J, Li C, Wolcott NS, Boone MH, Southern M, Kobzar NP, Salgado I. de A., Reddy DM, Sun F, et al. (2020). High-fat food biases hypothalamic and mesolimbic expression of consummatory drives. Nat. Neurosci 23, 1253–1266. 10.1038/s41593-020-0684-9. [PubMed: 32747789]
54. Canteras NS, and Swanson LW (1992). The dorsal premammillary nucleus: an unusual component of the mammillary body. Proc. Natl. Acad. Sci. U. S. A 89, 10089–10093. 10.1073/pnas.89.21.10089. [PubMed: 1279669]
55. Wang D, He X, Zhao Z, Feng Q, Lin R, Sun Y, Ding T, Xu F, Luo M, and Zhan C (2015). Whole-brain mapping of the direct inputs and axonal projections of POMC and AgRP neurons. Front. Neuroanat 9, 40. 10.3389/fnana.2015.00040. [PubMed: 25870542]
56. Vertes RP, and Hoover WB (2008). Projections of the paraventricular and paratenial nuclei of the dorsal midline thalamus in the rat. J. Comp. Neurol 508, 212–237. 10.1002/cne.21679. [PubMed: 18311787]
57. Berrios J, Li C, Madara JC, Garfield AS, Steger JS, Krashes MJ, and Lowell BB (2021). Food cue regulation of AGRP hunger neurons guides learning. Nature 595, 695–700. 10.1038/s41586-021-03729-3. [PubMed: 34262177]
58. Garfield AS, Shah BP, Burgess CR, Li MM, Li C, Steger JS, Madara JC, Campbell JN, Kroeger D, Scammell TE, et al. (2016). Dynamic GABAergic afferent modulation of AgRP neurons. Nat. Neurosci 19, 1628–1635. 10.1038/nn.4392. [PubMed: 27643429]
59. Higginson AD, Fawcett TW, Trimmer PC, McNamara JM, and Houston AI (2012). Generalized optimal risk allocation: foraging and antipredator behavior in a fluctuating environment. Am. Nat 180, 589–603. 10.1086/667885. [PubMed: 23070320]
60. Burnett CJ, Li C, Webber E, Tsaousidou E, Xue SY, Brüning JC, and Krashes MJ (2016). Hunger-Driven Motivational State Competition. Neuron 92, 187–201. 10.1016/j.neuron.2016.08.032. [PubMed: 27693254]
61. Burnett CJ, Funderburk SC, Navarrete J, Sabol A, Liang-Guallpa J, Desrochers TM, and Krashes MJ (2019). Need-based prioritization of behavior. eLife 8, e44527. 10.7554/eLife.44527. [PubMed: 30907726]

62. Atasoy D, Betley JN, Su HH, and Sternson SM (2012). Deconstruction of a neural circuit for hunger. Nature 488, 172–177. 10.1038/nature11270. [PubMed: 22801496]

63. Garfield AS, Li C, Madara JC, Shah BP, Webber E, Steger JS, Campbell JN, Gavrilova O, Lee CE, Olson DP, et al. (2015). A neural basis for melanocortin-4 receptor-regulated appetite. Nat. Neurosci 18, 863–871. 10.1038/nn.4011. [PubMed: 25915476]

64. Li X-Y, Han Y, Zhang W, Wang S-R, Wei Y-C, Li S-S, Lin J-K, Yan J-J, Chen A-X, Zhang X, et al. (2019). AGRP Neurons Project to the Medial Preoptic Area and Modulate Maternal Nest-Building. J. Neurosci. Off. J. Soc. Neurosci 39, 456–471. 10.1523/JNEUROSCI.0958-18.2018.

65. Alhadeff AL, Su Z, Hernandez E, Klima ML, Phillips SZ, Holland RA, Guo C, Hantman AW, De Jonghe BC, and Betley JN (2018). A Neural Circuit for the Suppression of Pain by a Competing Need State. Cell 173, 140–152.e15. 10.1016/j.cell.2018.02.057. [PubMed: 29570993]

66. Butler RK, Oliver EM, Sharko AC, Parilla-Carrero J, Kaigler KF, Fadel JR, and Wilson MA (2016). Activation of corticotropin releasing factor-containing neurons in the rat central amygdala and bed nucleus of the stria terminalis following exposure to two different anxiogenic stressors. Behav. Brain Res 304, 92–101. 10.1016/j.bbr.2016.01.051. [PubMed: 26821289]

67. Chen L, Cai P, Wang R-F, Lu Y-P, Chen H-Y, Guo Y-R, Huang S-N, Hu L-H, Chen J, Zheng Z-H, et al. (2020). Glutamatergic lateral hypothalamus promotes defensive behaviors. Neuropharmacology 178, 108239. 10.1016/j.neuropharm.2020.108239. [PubMed: 32771529]

68. Jennings JH, Sparta DR, Stamatakis AM, Ung RL, Pleil KE, Kash TL, and Stuber GD (2013). Distinct extended amygdala circuits for divergent motivational states. Nature 496, 224–228. 10.1038/nature12041. [PubMed: 23515155]

69. Jennings JH, Rizzi G, Stamatakis AM, Ung RL, and Stuber GD (2013). The inhibitory circuit architecture of the lateral hypothalamus orchestrates feeding. Science 341, 1517–1521. 10.1126/science.1241812. [PubMed: 24072922]

70. Jennings JH, Ung RL, Resendez SL, Stamatakis AM, Taylor JG, Huang J, Veleta K, Kantak PA, Aita M, Shilling-Scrivo K, et al. (2015). Visualizing hypothalamic network dynamics for appetitive and consummatory behaviors. Cell 160, 516–527. 10.1016/j.cell.2014.12.026. [PubMed: 25635459]

71. Li Y, Zeng J, Zhang J, Yue C, Zhong W, Liu Z, Feng Q, and Luo M (2018). Hypothalamic Circuits for Predation and Evasion. Neuron 97, 911–924.e5. 10.1016/j.neuron.2018.01.005. [PubMed: 29398361]

72. Nieh EH, Matthews GA, Allsop SA, Presbrey KN, Leppla CA, Wichmann R, Neve R, Wildes CP, and Tye KM (2015). Decoding neural circuits that control compulsive sucrose seeking. Cell 160, 528–541. 10.1016/j.cell.2015.01.003. [PubMed: 25635460]

73. Xu H-Y, Liu Y-J, Xu M-Y, Zhang Y-H, Zhang J-X, and Wu Y-J (2012). Inactivation of the bed nucleus of the stria terminalis suppresses the innate fear responses of rats induced by the odor of cat urine. Neuroscience 221, 21–27. 10.1016/j.neuroscience.2012.06.056. [PubMed: 22766237]

74. Nguyen KP, O'Neal TJ, Bolonduro OA, White E, and Kravitz AV (2016). Feeding Experimentation Device (FED): A flexible open-source device for measuring feeding behavior. J. Neurosci. Methods 267, 108–114. 10.1016/j.jneumeth.2016.04.003. [PubMed: 27060385]

75. Krashes MJ, Shah BP, Koda S, and Lowell BB (2013). Rapid versus delayed stimulation of feeding by the endogenously released AgRP neuron mediators GABA, NPY, and AgRP. Cell Metab. 18, 588–595. 10.1016/j.cmet.2013.09.009. [PubMed: 24093681]

Highlights

- Predator exposure induced physiological/behavioral changes contingent on threat level
- Diminishing conflict via internal or external perturbations shifted feeding strategies
- Predator addition or PMd^{Cck} activation inhibited AgRP neurons resulting in hypophagia
- Increased caloric need via AgRP→BNST and/or LH enhanced food-seeking under predation

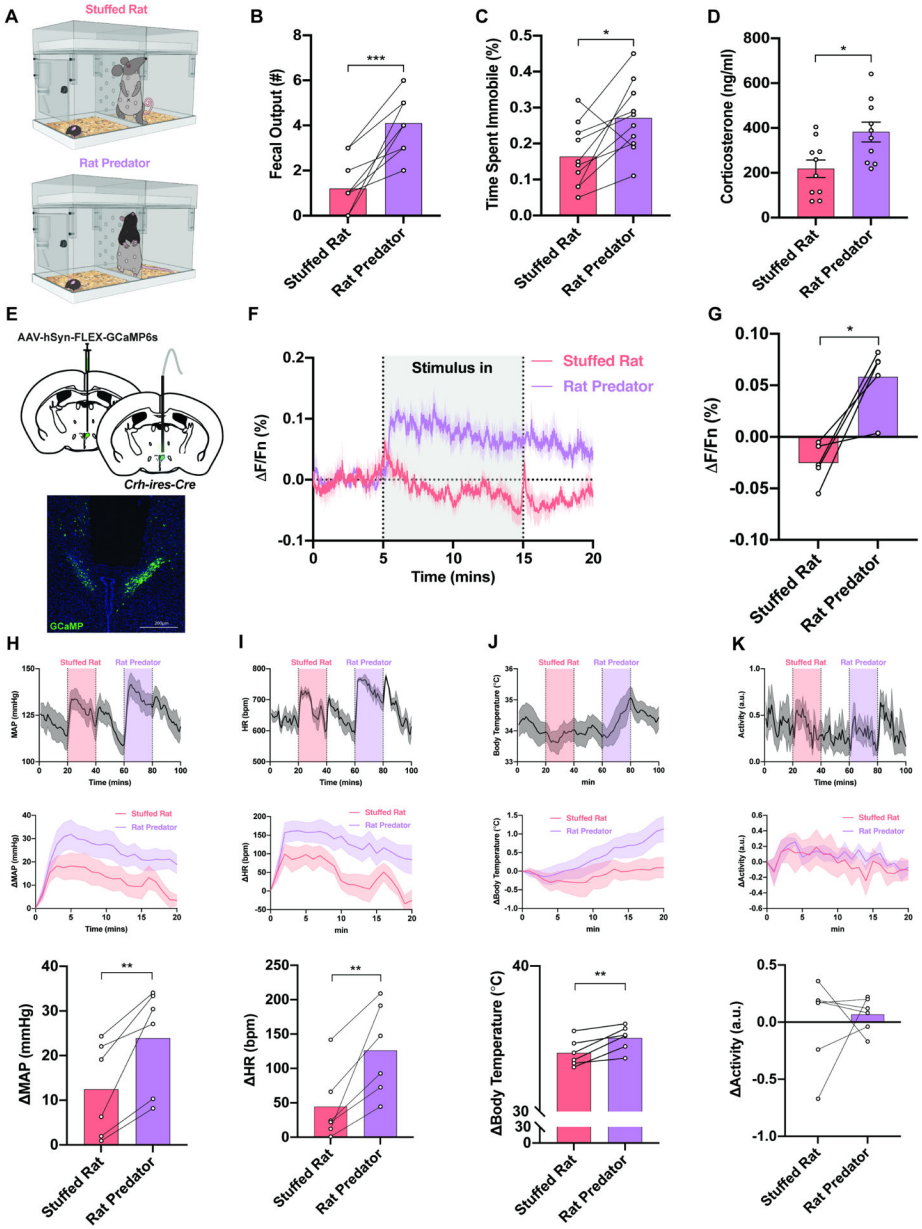

Figure 1. Rat predator stimulus evokes physiological, behavioral, and neuronal changes in mice.

A. Graphic of cage where mice are presented with a (Top) stuffed rat or (Bottom) rat predator. **B-D.** Rat predator exposure increased (B) fecal output, (C) time spent immobile and (D) blood corticosterone levels compared to a stuffed rat (n=10). **E.** (Top) Brain schematic of fiber photometry surgery whereby *Crh*-iresCre animals were unilaterally injected with Cre-dependent GCaMP6s virus in the PVH and unilaterally implanted with an optical fiber over the PVH. (Bottom) Representative image of GCaMP6s expression in PVH^{Crh} neurons. **F.** Average photometry traces under stuffed rat and rat predator conditions. **G.** Withinsubject quantification of PVH^{Crh} population response to stuffed rat and rat predator exposure (n=5). **H-K.** Rat predator exposure increased (H) MAP, (I) HR and (J) Tb

but had no effect on (K) physical activity compared to a stuffed rat (n=6). In all figures, *p < 0.05, **p < 0.01, ***p < 0.001 bars and error bars represent the mean ± SEM.

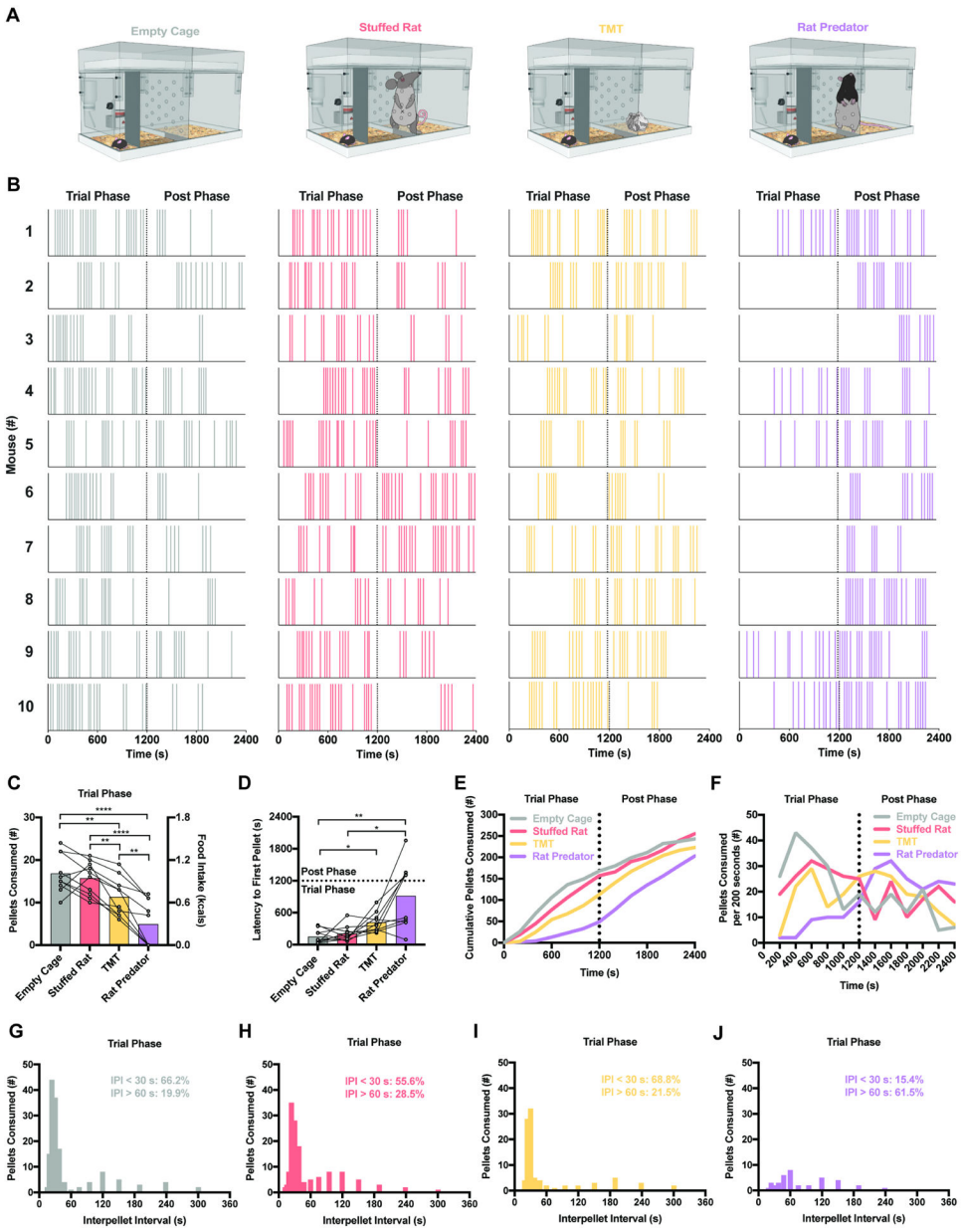

Figure 2. Rat predator exposure reduces food-seeking and consumption in hungry mice.

A. Graphic of cage used to evaluate behavior equipped with Feeding Experimental Device (FED), hide wall and water bottle. Adjoining cage is empty, containing a stuffed rat, TMT, or a rat predator. **B.** Raster plots of secondto-second food retrieval events during Trial and Post Phases (separated by black dotted line) across conditions. **C-J.** Rat predator exposure robustly (C) attenuates total food intake, (D) increases latency to retrieve the first pellet and blunts both (E-F) the rate of feeding and (G-J) inter-pellet interval between pellet retrieval and consumption (n=10). In all figures, *p < 0.05, **p < 0.01, ***p < 0.001 bars and error bars represent the mean ± SEM.

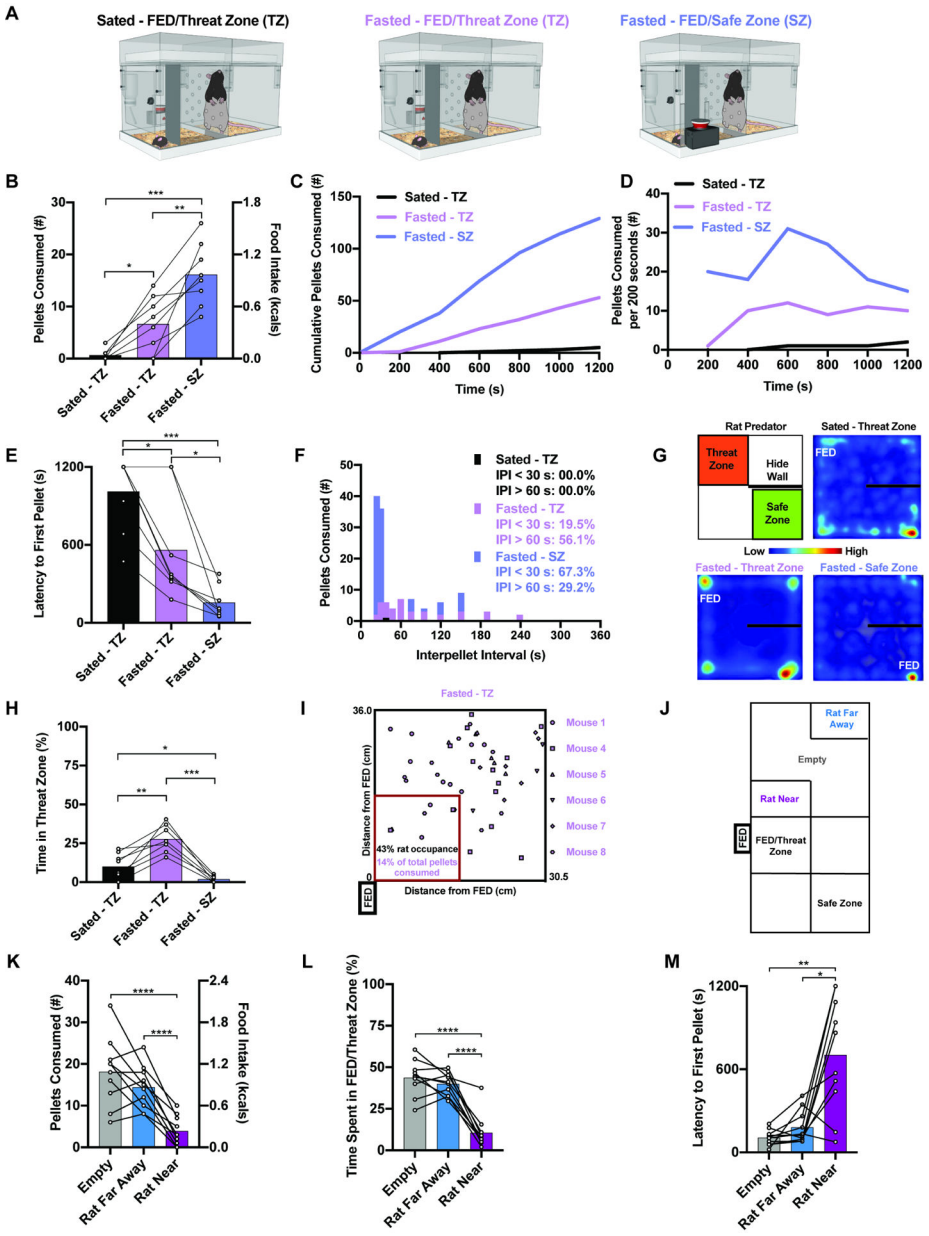

Figure 3. Diminishing conflict alters feeding behavior.

A. Graphic of cage used to evaluate behavior whereby the FED is located in either the Threat Zone (TZ) or Safe Zone (SZ). **B-F.** Safe Zone positioning of the FED escalates (B) total food intake and (C-D) rate of feeding while reducing (E) the latency to initiate feeding and (F) inter-pellet interval between pellet retrieval and consumption (n=8). **G.** Cage position schematic and average heat maps signifying the spatial position of mice across conditions. **H.** Hungry mice tasked with food-seeking in the Threat Zone spend a greater amount of time in the Threat Zone quadrant compared to the other conditions (n=8). **I-J.** Rat cage position schematic highlighting the rat snout location during individual pellet retrieval from the FED located in the Threat Zone for each mouse that consumed food. Red square signifies quadrant nearest to the FED occupied by the rat 43% of the entire trial time

across experiments. Notably, only 14% of all pellets consumed by mice are done when the rat occupies this quadrant. **(J-M)** Positioning of the rat nearest to the FED (J) diminishes (K) total food intake and (L) time spent in the FED/Threat Zone while increasing (M) the latency to initiate feeding compared to positioning of the rat farthest from the FED or an empty adjacent cage (n=10). In all figures, *$p < 0.05$, **$p < 0.01$, ***$p < 0.001$ bars and error bars represent the mean ± SEM.

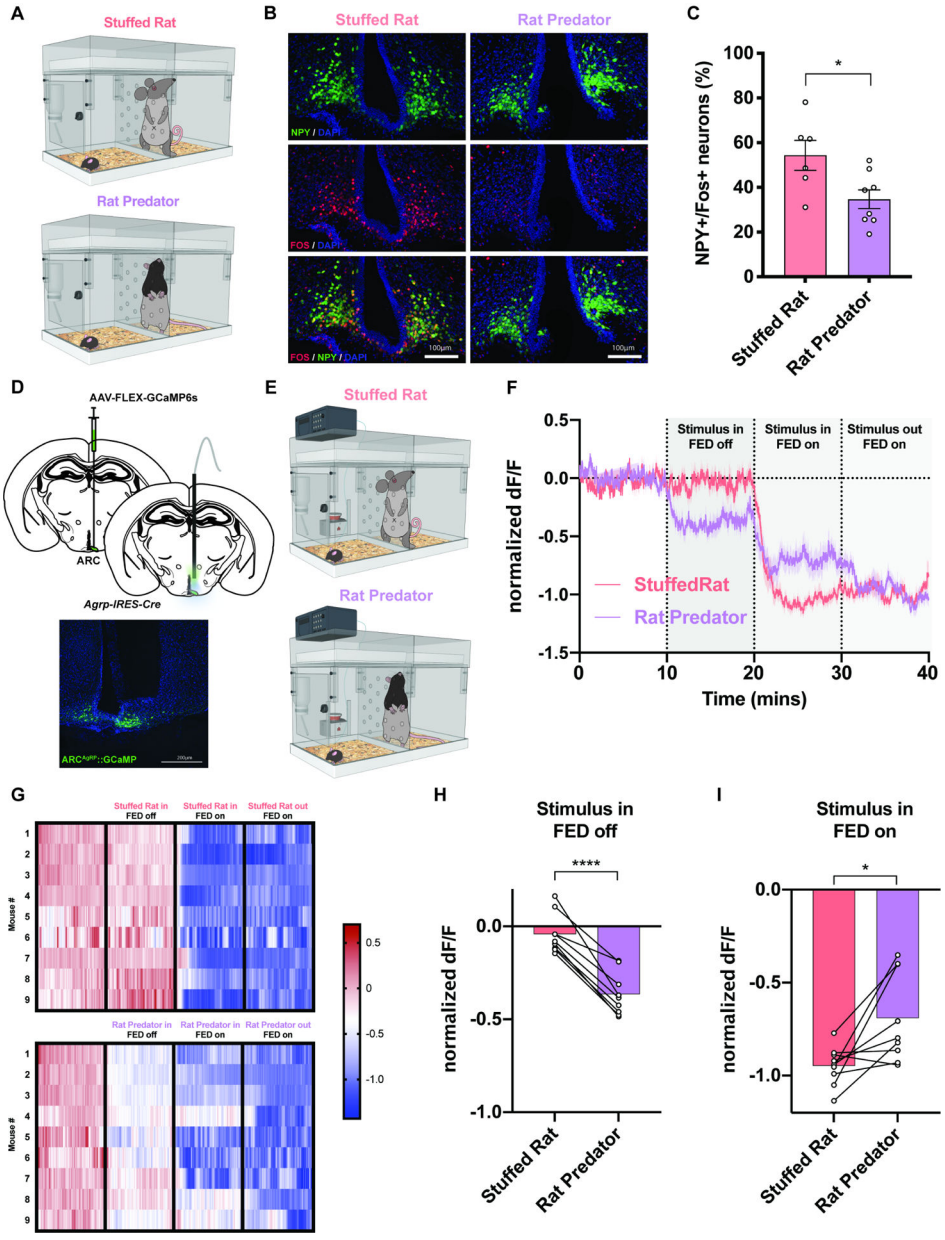

Figure 4. AgRP activity is rapidly blunted during rat predator presentation.

A. Graphic of cage used to assess Fos activity. **B-C.** Representative (B) images and (C) quantification demonstrating rat predator exposure lowers overlap between NPY and Fos expression in hungry mice compared to a stuffed rat (n=6 stuffed rat, n=8 rat predator). **D.** (Top) Brain schematic of fiber photometry surgery whereby *Agrp*-ires-Cre animals were unilaterally injected with Cre-dependent GCaMP6s virus in the ARC and unilaterally implanted with an optical fiber over the ARC. (Bottom) Representative image of GCaMP6s expression in AgRP neurons. **E.** Graphic of cage used to evaluate AgRP population activity. **F.** Average photometry traces aligned to 1) introduction of either the stuffed rat or rat predator (dotted line at 10 mins), 2) turning on the feeding device (2nd dotted line at 20 mins), and 3) removal of either the stuffed rat or rat predator (3rd dotted line at 30

mins). **G.** Corresponding heat maps of each individual animal under these conditions. **H.** Withinsubject quantification of AgRP population response demonstrating rat predator exposure suppresses AgRP activity compared to a stuffed rat (n=9). **I.** Within-subject quantification of AgRP population response to food during stuffed rat versus rat predator exposure (n=9). In all figures, *p < 0.05, **p < 0.01, ***p < 0.001 bars and error bars represent the mean ± SEM.

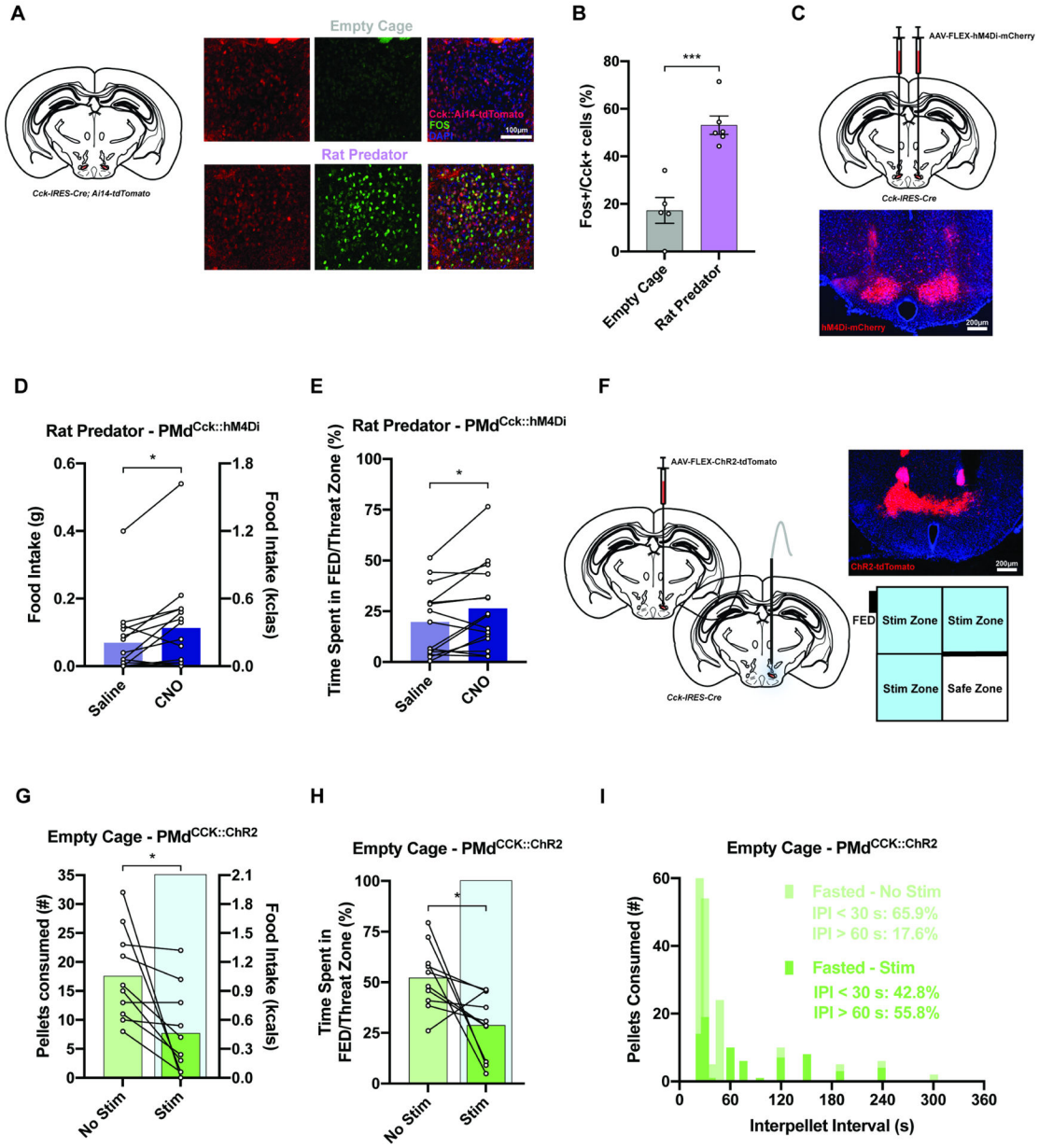

Figure 5. PMd^{Cck} neurons respond to a rat predator and gate feeding behavior under threat.

A. Brain schematic and representative images of *Cck*-ires-Cre; *Ai14-tdTomato* animals examining expression of Fos activity in response to a rat predator versus an empty cage in the PMd. **B.** Quantification showing elevated Fos expression in PMd^{Cck} neurons in the rat predator condition compared to an empty cage (n=5 empty cage, n=6 rat predator). **C.** (Top) Brain schematic of chemogenetic surgery whereby *Cck*-ires-Cre animals were bilaterally injected with Cre-dependent hM4Di virus in the PMd. (Bottom) Representative image of hM4Di expression in PMd^{Cck} neurons. **D-E.** Silencing of PMd^{Cck} neurons in hungry mice increased (D) food intake and (E) time spent in the FED/Threat Zone in the presence of a rat predator compared to withinsubject controls (n=15). **F.** (Left) Brain schematic of optogenetic surgery whereby *Cck*-ires-Cre animals were unilaterally injected with Cre-dependent ChR2

virus in the PMd and unlaterally implanted with an optical fiber over the PMd. (Middle) Representative image of ChR2 expression in PMd^{Cck} neurons. (Right) Schematic of closed-loop optogenetic arena. **G-I.** Activation of PMd^{Cck} neurons in hungry mice decreased (G) food intake and (H) time spent in the FED/Threat Zone and increased (I) inter-pellet interval between pellet retrieval and consumption compared to within-subject controls. Blue background indicates photoactivation (n=10). In all figures, *$p < 0.05$, **$p < 0.01$, ***$p < 0.001$ bars and error bars represent the mean ± SEM.

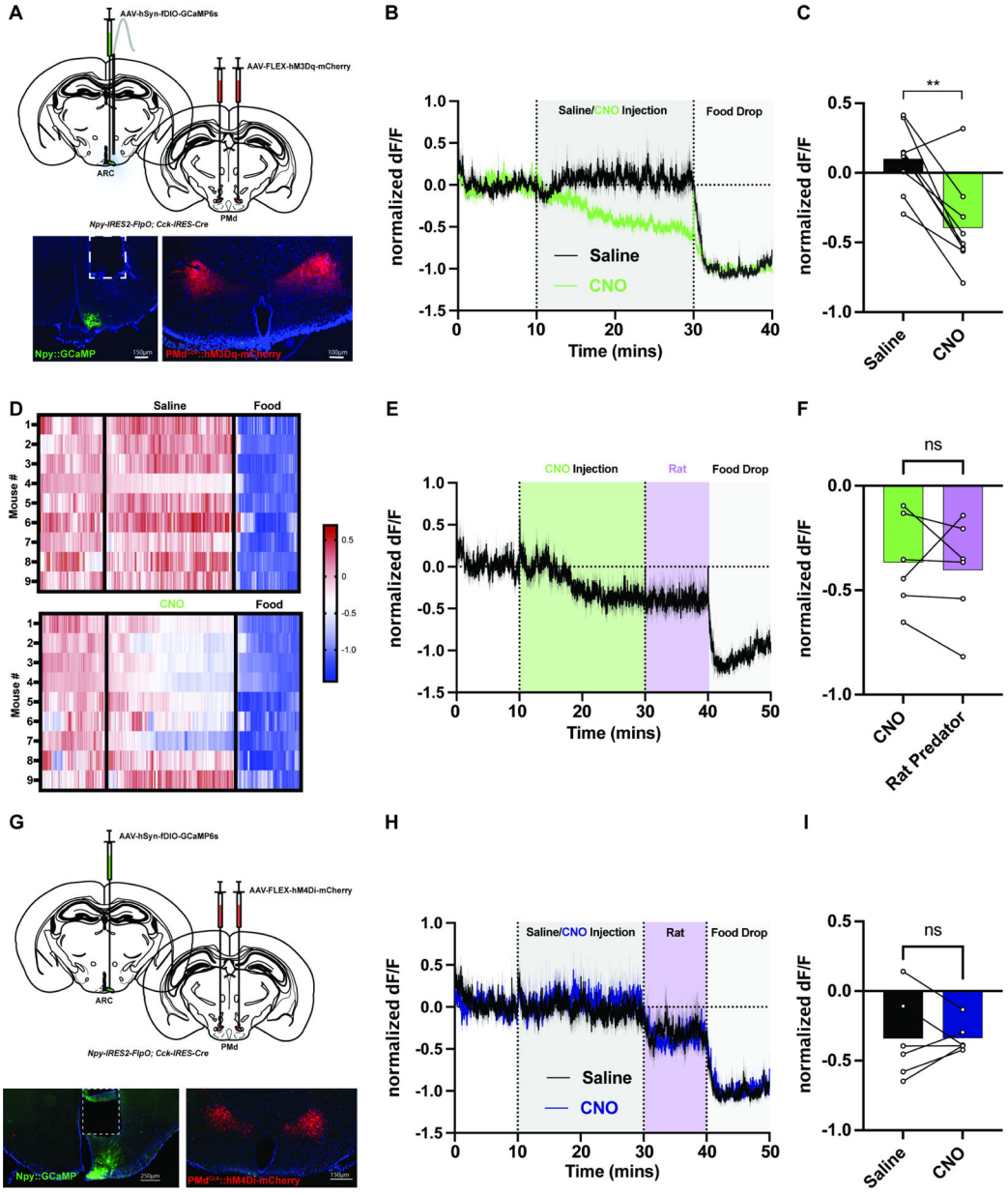

Figure 6. PMd^{Cck} neurons gate feeding behavior through AgRP/Npy inhibition.

A. (Top) Brain schematic of chemogenetic/fiber photometry surgery whereby *Cck*-ires-Cre; *Npy*-ires2-FlpO animals were bilaterally injected with a Cre-dependent hM3Dq virus in the PMd, unilaterally injected with a FlpOdependent GCaMP6 virus in the ARC, and unilaterally implanted with an optical fiber over the ARC. (Bottom) Representative image of hM3Dq expression in PMd^{Cck} neurons and GCaMP6 expression in AgRP/Npy neurons. **B.** Average photometry traces aligned to 1) saline or CNO injection (dotted line at 10 mins) and 2) food presentation (2nd dotted line at 30 mins). **C.** Within-subject quantification of AgRP/Npy population response after saline versus CNO injection showing activation of PMd^{Cck} neurons acutely suppresses AgRP/Npy activity (n=9). **D.** Corresponding heat maps of each individual animal under these conditions. **E.** Average photometry traces aligned to

1) CNO injection (dotted line at 10 mins), 2) rat predator presentation (2nd dotted line at 30 mins) and 3) food presentation (3rd dotted line at 40 mins). **F.** Withinsubject quantification of AgRP/Npy population response after CNO injection followed by rat predator presentation showing the suppression of AgRP/Npy activity via PMd^{Cck} stimulation is not further reduced by rat predator introduction (n=6). **G.** (Top) Brain schematic of chemogenetic/fiber photometry surgery whereby *Cck*-ires-Cre; *Npy*-ires2-FlpO animals were bilaterally injected with a Cre-dependent hM4Di virus in the PMd, unilaterally injected with a FlpO-dependent GCaMP6 virus in the ARC, and unilaterally implanted with an optical fiber over the ARC. (Bottom) Representative image of hM4Di expression in PMd^{Cck} neurons and GCaMP6 expression in AgRP/Npy neurons. **H.** Average photometry traces aligned to 1) saline or CNO injection (dotted line at 10 mins), 2) rat predator presentation (2nd dotted line at 30 mins) and 3) food presentation (dotted line at 40 mins). **I.** Within-subject quantification of AgRP/Npy population response after saline/CNO injection followed by rat predator presentation showing PMd^{Cck} inhibition does not affect the rat predator-evoked suppression of AgRP/Npy activity (n=6). In all figures, *$p < 0.05$, **$p < 0.01$, ***$p < 0.001$ bars and error bars represent the mean ± SEM.

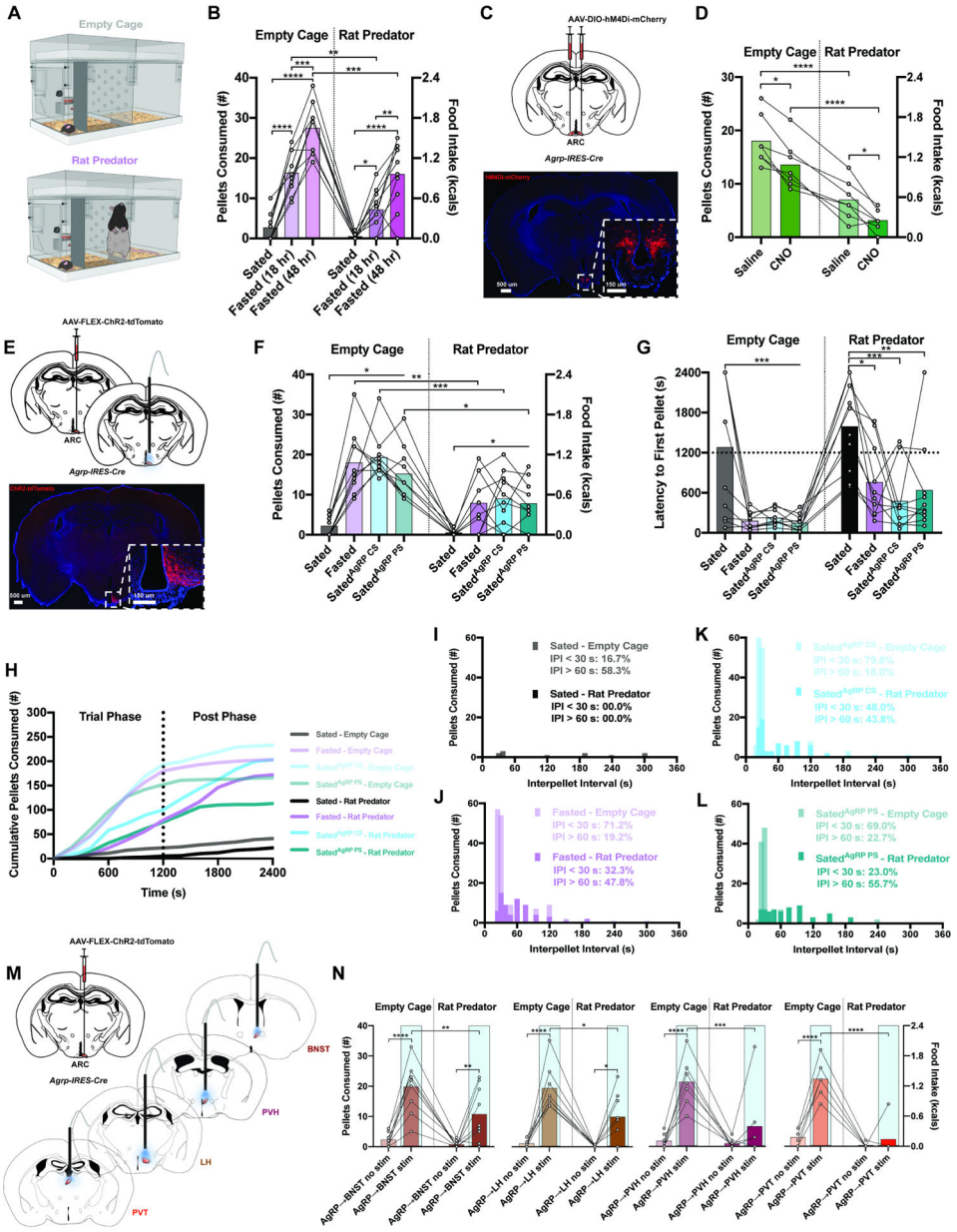

Figure 7. Feeding behavior under threat is scalable by internal state and mediated by AgRP neurons.

A. Graphic of cage used to evaluate behavior under varying degrees of physiological and artificial hunger. **B.** Lengthening period of caloric deprivation escalates food intake in both empty cage and rat predator conditions (n=10). **C.** (Top) Brain schematic of chemogenetic surgery whereby *Agrp*-ires-Cre animals were bilaterally injected with Cre-dependent hM4Di virus in the ARC. (Bottom) Representative image of hM4Di expression in AgRP neurons. **D.** Silencing of AgRP neurons in hungry mice reduces food intake in both empty cage and rat predator conditions (n=7). **E.** (Top) Brain schematic of optogenetic surgery whereby *Agrp*-ires-Cre animals were unilaterally injected with Cre-dependent ChR2 virus in the ARC and unlaterally implanted with an optical fiber over the ARC. (Bottom) Representative image of ChR2 expression in AgRP neurons. **F-H.** Both concurrent and preactivation of

AgRP neurons (F) increases food intake, (G) decreases latency to initiate eating, and (H) augments feeding rate comparable to within-subject hungry mice in both empty cage and rat predator conditions (n=10). **I-L.** Rat predator exposure robustly blunts inter-pellet interval between pellet retrieval and consumption compared to empty cage condition under both physiological and artificial hunger. **M.** Brain schematic of optogenetic surgery whereby *Agrp*-ires-Cre animals were unilaterally injected with Cre-dependent ChR2 virus in the ARC and unlaterally implanted with an optical fiber over the BNST, PVH, LH or PVT. **N.** Activation of AgRP terminal fields in the BNST, LH, PVH and PVT promote food intake in the empty cage condition but only AgRP projections to the BNST and LH stimulate food intake during rat predator exposure (n=9 AgRP→BNST, n=8 AgRP→LH, n=7 AgRP→PVH, n=6 AgRP→PVT). In all figures, *p < 0.05, **p < 0.01, ***p < 0.001 bars and error bars represent the mean ± SEM.

KEY RESOURCES TABLE

REAGENT or RESOURCE	SOURCE	IDENTIFIER
Antibodies		
Rabbit monoclonal anti-cFOS	Millipore Sigma	Cat#ABE457, RRID:AB_2631318
Donkey anti-rabbit-AlexaFluor488	Thermo Fisher Scientific	Cat# A32790, RRID:AB_2762833
Donkey anti-rabbit-AlexaFluor594	Thermo Fisher Scientific	Cat# A-21207, RRID:AB_141637
Bacterial and virus strains		
AAV9-CAG-Flex-ChR2-tdTomato	Atasoy et al., 2008.	Addgene, Cat#18917-AAV9
pAAV-CAG-DIO-ChR2(H134R)-eYFP	Rajendran et al., 2014.	Addgene, Cat#127090-PHPeB
pAAV9-hsyn-DIO-hM3dq-mcherry	Krashes et al., 2011	Addgene, Cat#44361-AAV9
pAAV9-hsyn-DIO-hM4di-mcherry	Krashes et al., 2011	Addgene, Cat#44362-AAV9
pAAV.Syn.Flex.GCaMP6s.WPRE.SV40	Chen et al., 2013	Addgene, Cat#100845-AAV1
AAV1-CAG-FLEX-X-jG-GCaMP7s-WPRE	Dana et al., 2019	Addgene, Cat#104495-AAV1
AAV8-EF1a-fDIO-gcamp6s	gift from Rylan Larsen	Addgene plasmid # 105714; RRID:Addgene_105 714
Chemicals, peptides, and recombinant proteins		
Clozapine N-oxide	Gift from Bryan Roth	NA
Vectashield Antifade Mounting Medium	Vector Laboratories	Cat#H-1000
Saline	Medline	DYND1000
4-hydroxytamoxifen	Sigma-Aldrich	Cat#H6278
2,3,5-trimethyl-3-thiazoline (TMT)	Contech Enterprises Inc	NA
DMSO	Sigma-Aldrich	Cat#472301
Tetrodotoxin	Abcam	Ab120055
4-aminopyridine	Abcam	Ab120122
Experimental models: Organisms/strains		
Crh-ires-Cre	Krashes et al., 2014. Gift from Dr. Bradford Lowell	
Agrp-ires-Cre	The Jackson Laboratory	*Agrp*$^{tm1(cre)Lowl}$/J Strain #:012899 RRID:IMSR_JAX:01 2899
Npy-hrGFP	The Jackson Laboratory	B6.FVB-Tg(Npy-hrGFP)1Lowl/J Strain #:006417 RRID:IMSR_JAX:00 6417
Cck-ires-Cre	The Jackson Laboratory	STOCK *Cck*$^{tm1.1(cre)Zjh}$/J Strain #:012706 RRID:IMSR_JAX:01 2706
Npy-ires2-FlpO	The Jackson Laboratory	B6.Cg-$^{Npytm1.1(flpo)Hze}$/J Strain #:030211 RRID:IMSR_JAX:03 021
NPY KO	The Jackson Laboratory	129S-Npy^{tm1Rpa}/J Strain #:004545 RRID:IMSR_JAX:00 4545

REAGENT or RESOURCE	SOURCE	IDENTIFIER
Ai14	The Jackson Laboratory	B6;129S6-Gt(ROSA)26Sor$^{tm14(C\ AG-tdTomato)Hze}$/J Strain #:007908 RRID:IMSR_JAX:00 7908
Fos$^{2A-iCreER}$	The Jackson Laboratory	STOCK *Fos$^{tm2.1(icre/E\ RT2)Luo}$*/J Strain #:030323 RRID:IMSR_JAX:030323
C57BL/6J	The Jackson Laboratory	Strain #:000664 RRID:IMSR JAX:00 0664
Long-Evans Rat	Charles River	Strain Code 006
Software and algorithms		
Ethovision XT16	Noldus	http://www.noldus.com; RRID:SCR 000441
Image J	Fiji	https://imagej.nih.gov/ij/
QuPath	Bankhead et al., 2017	https://qupath.github.io/
GraphPad Prism 8	GraphPad Software	https://www.graphpad.com/ RRID:SCR 002798
FEDviz	Matikainen-Ankney et al., 2021	https://github.com/earnestt1234/FED3_Viz
pClamp11 (Clampfit/Clamp Ex)	Molecular Devices	https://www.moleculardevices.com/products/axon-patch-clamp-system/acquisition-and-analysis-software/pclamp-software-suite%23gref